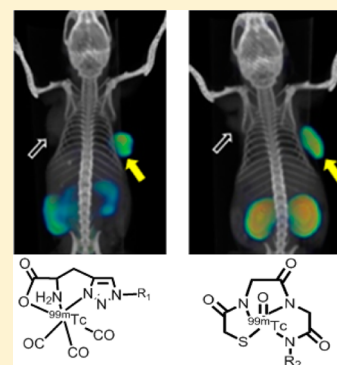


Effect of Chelators on the Pharmacokinetics of ^{99m}Tc -Labeled Imaging Agents for the Prostate-Specific Membrane Antigen (PSMA)Sangeeta Ray Banerjee,^{*,†} Mrudula Pullambhatla,[†] Catherine A. Foss,[†] Alexander Falk,[†] Youngjoo Byun,[‡] Sridhar Nimmagadda,[†] Ronnie C. Mease,[†] and Martin G. Pomper^{*,†}[†]Russell H. Morgan Department of Radiology and Radiological Science, Johns Hopkins University, School of Medicine, Baltimore, Maryland 21287, United States[‡]College of Pharmacy, Korea University, 2511 Sejong-ro, Jochiwon-eup, Yeongi-gun, Chungnam 339-700, South Korea

S Supporting Information

ABSTRACT: Technetium-99m, the most commonly used radionuclide in nuclear medicine, can be attached to biologically important molecules through a variety of chelating agents, the choice of which depends upon the imaging application. The prostate-specific membrane antigen (PSMA) is increasingly recognized as an important target for imaging and therapy of prostate cancer (PCa). Three different ^{99m}Tc -labeling methods were employed to investigate the effect of the chelator on the biodistribution and PCa tumor uptake profiles of 12 new urea-based PSMA-targeted radiotracers. This series includes hydrophilic ligands for radiolabeling with the $[\text{}^{99m}\text{Tc}(\text{CO})_3]^+$ core (L8–L10), traditional N_xS_y -based chelating agents with varying charge and polarity for the ^{99m}Tc -oxo core (L11–L18), and a ^{99m}Tc -organohydrazine-labeled radioligand (L19). $^{99m}\text{Tc}(\text{I})$ -Tricarbonyl-labeled $[\text{}^{99m}\text{Tc}]$ L8 produced the highest PSMA+ PC3 PIP to PSMA– PC3 flu tumor ratios and demonstrated the lowest retention in normal tissues including kidney after 2 h. These results suggest that choice of chelator is an important pharmacokinetic consideration in the development of ^{99m}Tc -labeled radiopharmaceuticals targeting PSMA.



INTRODUCTION

Technetium-99m (half-life, 6 h; γ -energy, 140.5 keV) is widely used in nuclear medicine because of its nearly ideal photon energy for single photon emission computed tomography (SPECT), low dose burden to the patient, low cost, ready availability, and synthetic tractability for incorporating into biological targeting agents. Despite the wide availability of PET isotopes (such as ^{18}F , $^{62/64}\text{Cu}$, and ^{68}Ga) in Western countries, ^{99m}Tc remains the radionuclide of choice for development of diagnostic radiotracers in most developing countries and is the most heavily utilized diagnostic medical isotope.¹ Adding further to its convenience, ^{99m}Tc -labeled biotargeting agents can be prepared via a commercially available kit. A variety of well-established chelating agents is available for incorporating ^{99m}Tc into biotargeting agents, however, the effects of various chelators and the composition of the ^{99m}Tc core (inherent functionalities attached to ^{99m}Tc) on the pharmacokinetics of the parent compounds have not been well characterized for specific indications.²

Prostate cancer (PCa) is the most commonly diagnosed malignancy with few options for molecular imaging due to its relatively low metabolism. Prostate-specific membrane antigen (PSMA), an integral membrane protein, is increasingly recognized as a viable target for imaging and therapy of PCa.^{3,4} Elevated expression of PSMA is associated with metastasis,⁵ androgen independence,⁶ and progression⁷ of PCa. We and others have previously demonstrated the ability

of radiohalogenated, urea-based, low-molecular-weight inhibitors of PSMA to image PSMA expression in prostate tumor xenografts.^{8,9} The SPECT agents $[\text{}^{123}\text{I}]\text{MIP-1072}$ and $[\text{}^{123}\text{I}]\text{MIP-1095}$ and the PET agent $[\text{}^{18}\text{F}]\text{DCFBC}$ have demonstrated promise by detecting both bone and lymph node metastases in clinical studies.^{10,11} Recently, we and others have extended that work to include the radiometal ^{99m}Tc via coordinated, $^{99m}\text{Tc}(\text{I})$ tricarbonyl,^{12–16} or $^{99m}\text{Tc}(\text{V})$ -oxo^{17,18} moieties. Generally, to retain binding affinity to PSMA, a linker was required between the PSMA-targeting moiety and the metal chelator.¹⁶ While changes in the linker are known to affect the biodistribution of these agents,^{16,17} the effect of various chelators and related ^{99m}Tc -labeled cores on the pharmacokinetics of compounds of this class have not been well characterized.

Here we expand upon our earlier work with urea-based, PSMA-targeted imaging agents to address the effect of various common chelators of ^{99m}Tc on the pharmacokinetics and tumor uptake in a small series of new imaging agents. Here we used three different ^{99m}Tc core complexes and related chelating agents for comparison: (1) $[\text{}^{99m}\text{Tc}(\text{CO})_3]^+$ core using a lysine-based tridentate chelator, demonstrated in $[\text{}^{99m}\text{Tc}]\text{L8–L10}$, (2) the ^{99m}Tc -oxo ($[\text{}^{99m}\text{TcO}]^{3+}$) core as in $[\text{}^{99m}\text{Tc}]\text{L11–L18}$, which is most frequently used for radiolabeling of biomolecules with ^{99m}Tc , and (3) ^{99m}Tc -organohydrazine $[\text{}^{99m}\text{TcNHNR}]^{2+}$ as

Received: April 6, 2013

Published: June 25, 2013

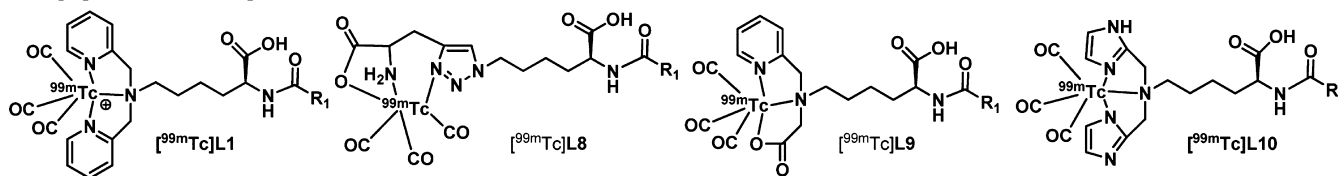
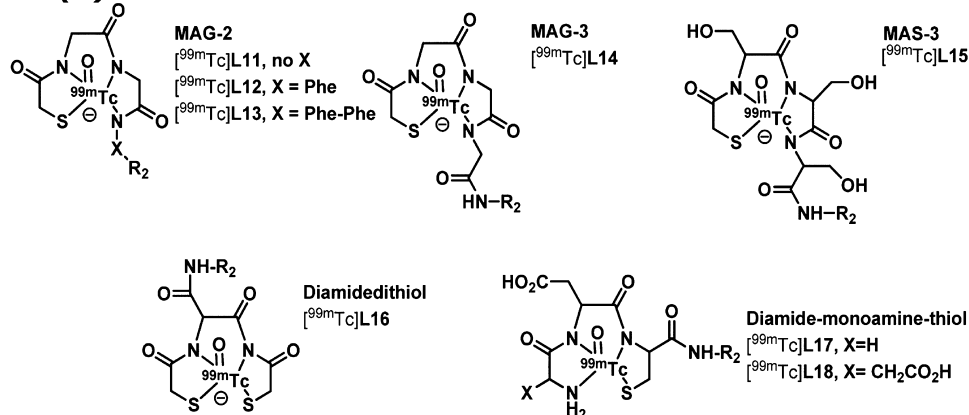
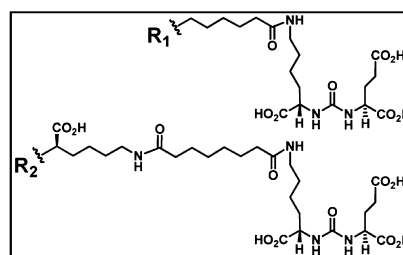
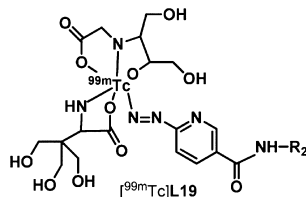
Tc(I) tricarbonyl**Tc(V) oxo****Tc(III) hynic**

Figure 1. ^{99m}Tc -Labeled inhibitors of PSMA.

in ^{99m}Tc L19, which is of particular interest due to its high ^{99m}Tc labeling efficiency (Figure 1). By altering the chelators for ^{99m}Tc , the compounds produced consequently demonstrated differences in overall charge, lipophilicity, stability, and affinity, which we reasoned would alter their pharmacokinetics. Additionally, we briefly investigated the effect of aromatic substituents in the linker moiety on pharmacokinetics.

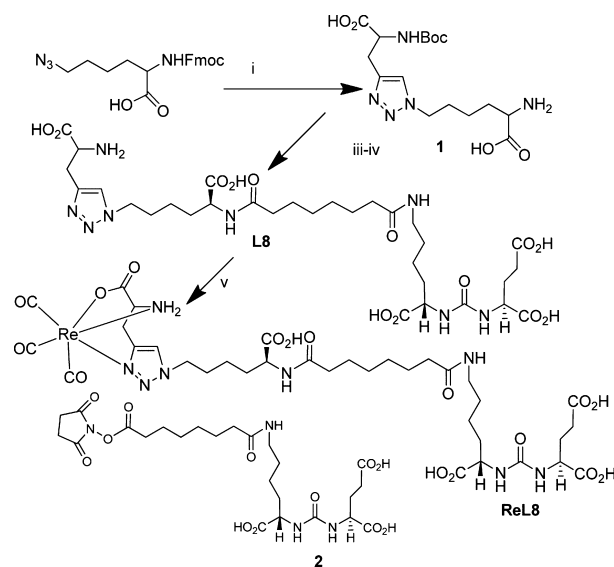
Imaging and biodistribution studies in NOD/SCID mice harboring PCa xenografts demonstrate that both tricarbonyl and ^{99m}Tc -oxo complexes have favorable pharmacokinetics over the HYNIC-conjugated compound. Between the tricarbonyl and ^{99m}Tc -oxo complexes, tricarbonyl complex ^{99m}Tc L8 exhibited superior tumor uptake and tumor-to-muscle and tumor-to-blood ratios that are suitable for clinical translation. Our studies also show that choice of chelating agent significantly affects the stability, affinity, lipophilicity, and ultimately pharmacokinetics of the final ^{99m}Tc -labeled radioligands, suggesting that these results may have implications in the synthesis of ^{99m}Tc -labeled imaging agents in general.

RESULTS

Chemical and Radiochemical Synthesis. Chemical and radiochemical syntheses are shown in Schemes 1–5. Compound L8 contains 1,4-disubstituted 1,2,3-triazole functionalized lysine as a chelating agent. ^{99m}Tc labeling of this class of triazole containing chelators has recently been developed by Schibli's group¹⁹ and was prepared through click chemistry^{20,21}

as shown in Scheme 1. In particular, a click reaction was performed between commercially available fluorenylmethox-

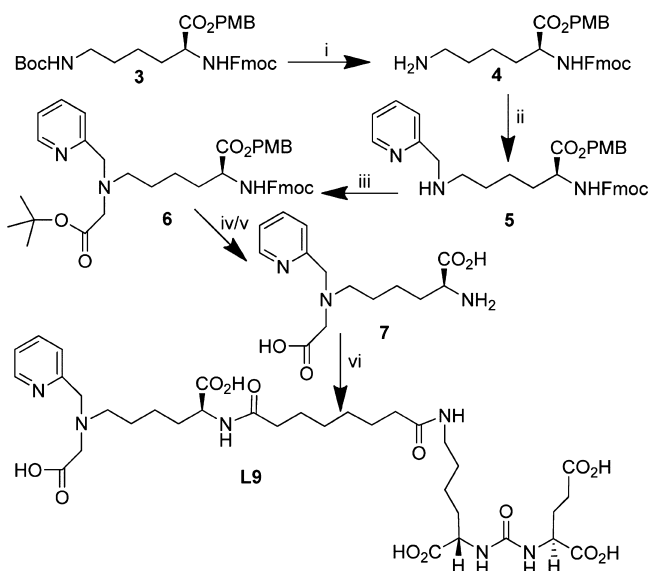
Scheme 1. Synthesis of L8 and ReL8^a



^a(i) *N*-Boc-propargylglycine, $\text{Cu}(\text{OAc})_2$, sodium ascorbate, $\text{H}_2\text{O}/t\text{-BuOH}$ (1:1), rt; (ii) 20% piperidine/DMF; (iii) 2, DMF, DIEA, rt; (iv) TFA/ CH_2Cl_2 /TES; (v) $[\text{Re}(\text{CO})_3(\text{H}_2\text{O})_3]\text{Br}$, $\text{MeOH}/\text{H}_2\text{O}$.

ycarbonyl (Fmoc)-Lys(azide)-OH and Boc-Gly-propargyl-OH in the presence of a catalytic amount of $\text{Cu}(\text{OAc})_2$ and sodium ascorbate and Tris-[(1-benzyl-1*H*-1,2,3-triazol-4-yl) methyl]-amine (TBTA) at ambient temperature followed by Fmoc removal to provide **1** in 45% yield. **L8** was obtained upon coupling of **1** with the NHS ester of urea-suberate **2**,²² followed by removal of the Boc group using TFA/ CH_2Cl_2 /triethylsilane (TES) (1/1/0.05) in ~60% yield. The rhenium tricarbonyl complex (**ReL8**) was synthesized by using $[\text{Re}(\text{CO})_3(\text{H}_2\text{O})_3]\text{Br}$ ²³ as shown in Scheme 1. The monopyridyl monoacid lysine chelating agent was prepared in a multistep synthesis as outlined in Scheme 2. The acid group of Fmoc-Lys(Boc)-

Scheme 2. Synthesis of L9^a

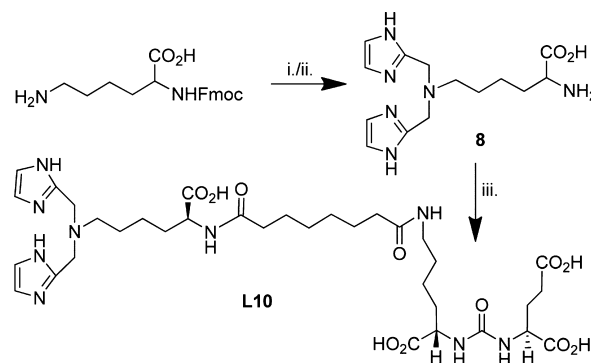


^a(i) TsOH, EtOH EtOAc, rt; (ii) py-2-aldehyde, $\text{NaBH}(\text{OAc})_3$, DCE, rt; (iii) *t*-butyl bromoacetate KI, DIEA, DMF; (iv) 20% piperidine/DMF; (v) TFA, CH_2Cl_2 , TIS; (vi) **2** DMF, DIEA.

CO_2H was protected using *p*-methoxy-benzyl chloride and Cs_2CO_3 to obtain **3** in 70% yield.¹⁶ Selective removal of the Boc group using *p*-toluenesulfonic acid in the presence of ethanol at ambient temperature provided **4** in 60% yield. Reductive amination of **4** with pyridine-2-aldehyde provided **5** in 40% yield. Alkylation of **5** by bromo-*t*-butyl-acetate at 25 °C produced **6** in moderate yield (33%). Removal of the Fmoc group by 20% piperidine/DMF followed by removal of the PMB groups and the *tert*-butyl group by TFA/ CH_2Cl_2 at 25 °C afforded the desired chelating agent **7**, which was reacted with **2** to produce **L9** in a yield of 60%. Compound **L10** was prepared in two steps as described in Scheme 3. Reductive amination of imidazole-2-aldehyde with Fmoc-Lys-OH in the presence of $\text{NaBH}(\text{OAc})_3$ and acetic acid followed by Fmoc removal provided chelating agent **8** in ~30% yield. Chelating agent **8** was reacted with **2** to provide the PSMA-targeting ligand **L10** in ~50% yield.

A generalized Fmoc-based solid phase peptide synthesis strategy was developed with a combination of solution phase chemistry as required to prepare ligands **L11**–**L18**. Commercially available Fmoc-Lys(Boc)-Wang resin was conjugated with required amino acid residues, after which the compound was cleaved from the resin by an ice-cold mixture of TFA/ CH_2Cl_2 /triethyl silane (TES) (1/1/0.01) for 1 h at ambient temperature. After isolating the resin cleaved product **9**, the

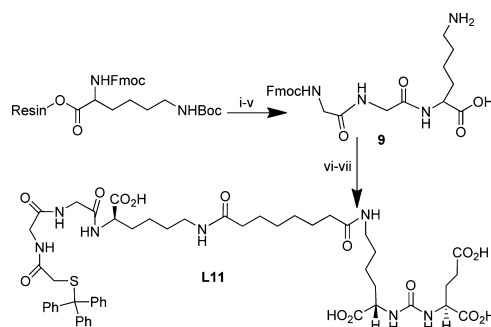
Scheme 3. Synthesis of L10^a



^a(i) Imidazole-2-aldehyde, $\text{NaBH}(\text{OAc})_3$, $\text{CH}_3\text{CO}_2\text{H}$, $\text{NaBH}(\text{OAc})_3$, dichloroethane; (ii) 20% piperidine/DMF; (iii) **2**, DIEA, DMF.

free ϵ -amine of lysine was then conjugated with **2**, followed by Fmoc removal and conjugation of the α -amine with the NHS ester of mercaptoacetic acid²⁴ to produce **L11** as shown in Scheme 4.

Scheme 4. Synthesis of L11^a

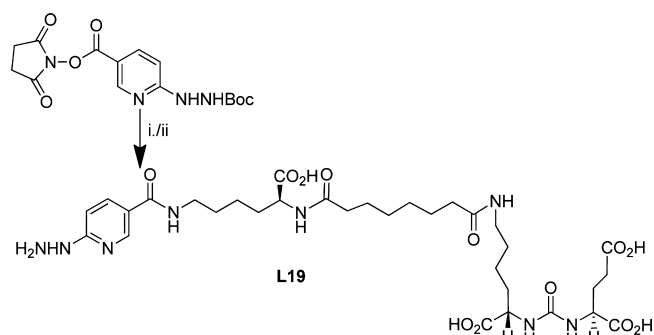


^a(i) 20% piperidine in DMF; (ii) Fmoc-Gly-OH, HBTU, HOBT, DIEA, DMF; (iii) 20% piperidine in DMF; (iv) Fmoc-Gly-OH, HBTU, HOBT, DIEA, DMF; (v) TFA/TIS/ CH_2Cl_2 ; (vi) **2**, DIEA, DMSO, rt; (vii) *S*-trityl- $\text{CH}_2\text{CO}_2\text{-NHS}$, DIEA, DMF.

Compound **L19** was generated through a well-established labeling approach using the HYNIC chelating agent (Scheme 5). Commercially available HYNIC(Boc)-NHS was conjugated to compound **10**,²⁵ to produce **L19** in 90% yield.

Radiotracers $[\text{}^{99\text{m}}\text{Tc}]\text{L8-L10}$ were synthesized as $^{99\text{m}}\text{Tc}(\text{CO}_3)$ complexes using the same general method as described

Scheme 5. Synthesis of L19^a



^a(i) **10**, DIEA, DMF; (ii) TFA/ CH_2Cl_2 /TIS.

previously by us for the preparation of [^{99m}Tc]L1 using the tricarbonyl labeling Isolink kit.¹⁶ These new radioligands were obtained in reasonable radiochemical yields (70–95%) and in high radiochemical purities (>98%) as determined by HPLC, with a specific activity >411 GBq/ μmol (1.1×10^4 mCi/ μmol) upon reaction with [$^{99m}\text{Tc}(\text{CO})_3$]⁺ at ligand concentrations of 10^{-6} M at 95 °C (boiling water bath) for 30 min.

Radiolabeling of L11–L18 was performed following a general literature procedure.²⁶ Ligands were dissolved in 0.5 M ammonium acetate with 5–10% DMSO and reacted with disodium tartrate and a solution of ascorbic acid and SnCl_2 , followed by addition of $^{99m}\text{TcO}_4^-$ and left at ~90–95 °C for 10–15 min. Radiolabeled products were obtained in >80% yield for all compounds, in >99% radiochemical purity with specific activity >411 GBq/ μmol (1.1×10^4 mCi/ μmol). Two radiolabeled peaks were isolated for all three MAG-2 conjugated radioligands [^{99m}Tc]L11, [^{99m}Tc]L12, and [^{99m}Tc]L13, whereas for all MAG-3 and MAS-3 conjugated radiotracers, only a single peak was isolated during radiolabeling. Interestingly, for all ligands except for L16, radiolabeling went smoothly using the S-trityl protected version of the ligand. Although both the protected and deprotected versions ultimately provide the same radiolabeled product, we used the protected starting materials to enable easier UV detection and separation by HPLC. A single set of HPLC conditions could be used to isolate radioligands [^{99m}Tc]L11–L18. Moreover, the S-trityl protected ligands proved stable in solution until subjected to radiolabeling conditions. Radiolabeling of the HYNIC adduct was performed according to a literature procedure by treating with tricine and SnCl_2 at ambient temperature for 30 min.²⁷

In Vitro Binding and Cell Uptake. All compounds demonstrated high binding affinity to PSMA with K_i values ranging from 0.03 to 16.30 nM (Table 1). We also synthesized

Table 1. PSMA Inhibitory Activity^a

compd	K_i	95% CI (K_i) (nM)
L8	1.12	0.10–11.62
ReL8	0.35	0.25–0.54
L9	12.60 ^a	10.46–15.20 ^a
L10	16.30 ^a	8.78–30.32 ^a
L11	0.03	0.02–0.06
L12	0.13	0.08–0.20
L13	1.91	1.54–2.37
L14	7.99	2.05–31.14
L15	0.18	0.10–0.32
L16	0.048	0.02–0.14
L17	0.17	0.11–0.30
L18	2.73	2.24–3.33
L19	1.74	0.96–3.17
ZJ43	0.43	0.31–0.62

^aSeparate experiment, ZJ43, (K_i 11.81 nM, 95% CI(10.31–13.53)).

an analogue of L8 that incorporates Re and observed a 3-fold improvement in binding affinity for ReL8 over L8 (Table 1). Comparative cell uptake involving [^{99m}Tc]L8 revealed ~100 fold higher uptake in PSMA+ PC3 PIP cells relative to PSMA– PC3 flu cells. This uptake in PIP cells could be blocked by treatment with 10 μmol of the known, high-affinity PSMA inhibitor, ZJ43 (Supporting Information Figure S1).²⁸

Small Animal SPECT-CT Imaging. Whole body SPECT-CT images were obtained for [^{99m}Tc]L8–L19 in male SCID

mice (Figures 2–4, Supporting Information Figures S2–S7) bearing PSMA+ PC3 PIP and PSMA– PC3 flu xenografts in opposite flanks at 2 h postinjection. Pharmacokinetics derived from the images were used to determine which compound(s) would be further evaluated in tissue biodistribution studies. Irrespective of charge and lipophilicity, radioligands [^{99m}Tc]L8–L18 enabled visualization of PSMA+ PC3 PIP tumor and the kidneys. Renal uptake of the radiotracers is partially due to their route of excretion as well as to specific uptake from the expression of PSMA in mouse proximal tubules.²⁹ In vivo images of the neutral complex, [^{99m}Tc]L8, were promising because of comparatively low background within the gastrointestinal tract and gallbladder compared to the previously published, positively charged compound, [^{99m}Tc]L1. SPECT-CT images acquired at 30 min, 2 and 6 h postinjection of [^{99m}Tc]L8 (Supporting Information Figure S2), showed clear PSMA+ PC3 PIP tumor uptake as early as 30 min postinjection. At 30 min and 2 h postinjection, the most visible tissues were PSMA+ PC3 PIP tumor and kidneys, with some accumulation of radioactivity observed in the liver, gallbladder, gastrointestinal tract, and urinary bladder. The radioactivity in the gallbladder and kidneys cleared significantly by 6 h, however, there was mild, residual retention of radioactivity within the gastrointestinal tract. Although [^{99m}Tc]L9 and [^{99m}Tc]L10 demonstrated high PSMA+ PC3 PIP tumor uptake, they also showed significant accumulation within gallbladder and the gastrointestinal tract at 2 h postinjection (Figure 2). Accordingly, [^{99m}Tc]L9 and [^{99m}Tc]L10 were considered to have provided inferior images compared to [^{99m}Tc]L8 and our previous lead compound, [^{99m}Tc]L1.¹⁶

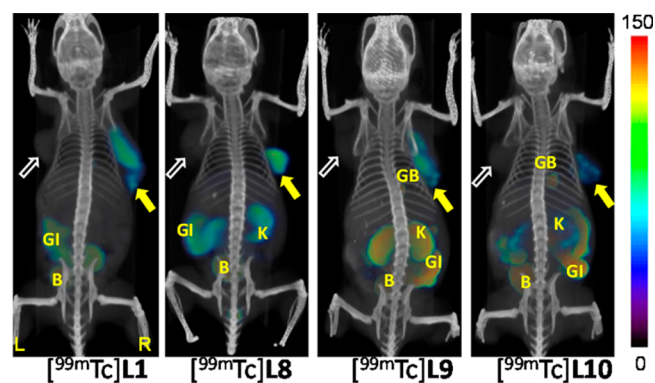


Figure 2. Whole body SPECT-CT imaging of PSMA+ PC3 PIP and PSMA– PC3 flu tumor-bearing mice with tricarbonyl compounds [^{99m}Tc]L8, [^{99m}Tc]L9, and [^{99m}Tc]L10 at 2 h postinjection, respectively. Mice were injected with ~37 MBq (1 mCi) of radiopharmaceutical IV. PIP = PC3 PSMA+ PC3 PIP (solid arrow), flu = PSMA– PC3 flu (unfilled arrow), GB = gallbladder, GI = gastrointestinal tract, K = kidney, B = bladder, L = left, R = right. All images are decay-corrected and adjusted to the same maximum scale.

SPECT-CT images of the negatively charged ^{99m}Tc -oxo-labeled radioligands [^{99m}Tc]L11–L15 (Figure 3) and [^{99m}Tc]L16 (Figure 4), and neutral radioligands [^{99m}Tc]L17 and [^{99m}Tc]L18 (Figure 4) demonstrated high radiotracer accumulation within PSMA+ PC3 PIP tumor and kidneys at 2 h postinjection. Furthermore, among [^{99m}Tc]L11, [^{99m}Tc]L15, and [^{99m}Tc]L18 (Figure 3, Supporting Information Figures S3, S4 and S6), retention of radioactivity within PSMA target sites

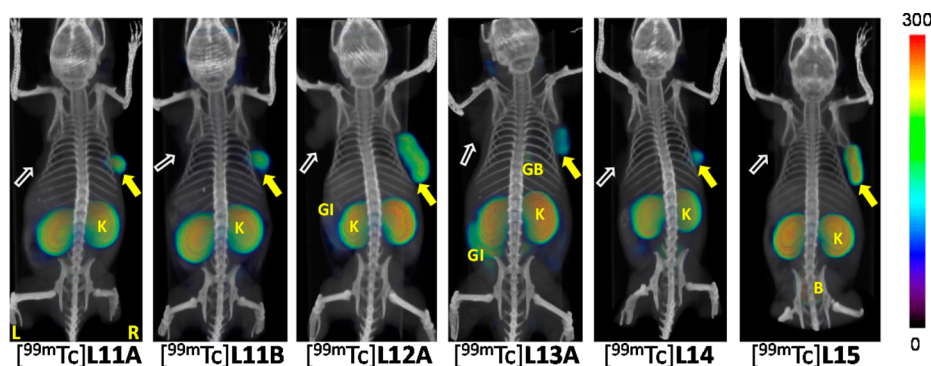


Figure 3. Whole-body SPECT-CT imaging of PSMA+ PC3 PIP and PSMA- PC3 flu tumor-bearing mice with [^{99m}Tc]L11A, [^{99m}Tc]L11B, [^{99m}Tc]L12A, [^{99m}Tc]L13A, [^{99m}Tc]L14, and [^{99m}Tc]L15 at 2 h postinjection, respectively. Mice were injected with ~ 37 MBq (1 mCi) of radiopharmaceutical IV. PIP = PSMA+ PC3 PIP (filled arrow), flu = PSMA- PC3 flu (unfilled arrow), GB = gallbladder, GI = gastrointestinal tract, K = kidney, B = bladder, L = left, R = right. All images are decay-corrected and adjusted to the same maximum scale.

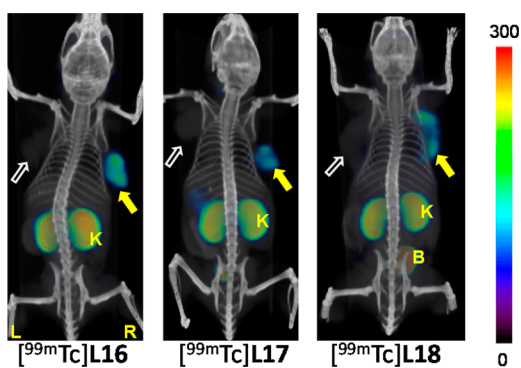


Figure 4. Whole body SPECT-CT imaging of PSMA+ PC3 PIP and PSMA- PC3 flu tumor-bearing mice with [^{99m}Tc]L16, [^{99m}Tc]L17, and [^{99m}Tc]L18 at 2 h postinjection, respectively. Mice were injected with ~ 37 MBq (1 mCi) of radiopharmaceutical IV. PIP = PSMA+ PC3 PIP (filled arrow), flu = PSMA- PC3 flu (unfilled arrow), K = kidney, B = bladder, L = left, R = right. All images are decay-corrected and adjusted to the same maximum scale.

was observed even at 18 h, suggesting the opportunity for protracted imaging using these agents.

As a further test of binding specificity, we imaged animals administered [^{99m}Tc]L11 after pretreating them with 50 mg/kg of ZJ43. ZJ43 proved capable of blocking the binding of [^{99m}Tc]L11 (Supporting Information Figure S5), not only within the tumor but also within the renal cortex and salivary glands, confirming that uptake observed in these tissues is PSMA-mediated.

Among the MAG-2-chelated ligands, L11–L13, which possess different lipophilicities due to the presence of zero, one, and two Phe residues on the linker, respectively, considerable differences in nontarget tissue uptake were observed for their radiolabeled counterparts (Figure 3). High gallbladder, liver, and gastrointestinal uptake were observed for [^{99m}Tc]L13 compared to [^{99m}Tc]L11. Also, as mentioned above, [^{99m}Tc]L11–L13 were obtained as two different diastereomers. Both radiolabeled isomers were investigated in SPECT imaging studies for [^{99m}Tc]L11 (Figure 3 and Supporting Information Figure S3). No significant difference was observed with respect to the tumor uptake, nontarget tissue uptake, or clearance between the isomeric compounds.

Table 2. Biodistribution of [^{99m}Tc]L8 in Tumor Bearing Mice^a

	0.5 h	1 h	2 h	5 h
blood	1.35 \pm 1.22	0.46 \pm 0.20	0.19 \pm 0.05	0.13 \pm 0.05
heart	0.65 \pm 0.26	0.52 \pm 0.23	0.22 \pm 0.14	0.08 \pm 0.01
lung	2.47 \pm 0.83	1.78 \pm 0.29	0.92 \pm 0.14	0.30 \pm 0.09
liver	28.85 \pm 17.93	11.36 \pm 1.57	6.11 \pm 0.66	3.24 \pm 0.39
stomach	0.73 \pm 0.16	0.41 \pm 0.21	0.17 \pm 0.05	0.20 \pm 0.13
pancreas	1.08 \pm 0.18	0.43 \pm 0.12	0.25 \pm 0.12	0.10 \pm 0.06
spleen	21.11 \pm 8.49	12.28 \pm 2.99	4.42 \pm 1.68	1.83 \pm 1.52
fat	1.08 \pm 0.49	0.66 \pm 0.06	0.33 \pm 0.12	0.12 \pm 0.04
kidney	122.70 \pm 14.73	119.15 \pm 0.01	116.2 \pm 14.2	55.31 \pm 1.15
muscle	0.71 \pm 0.27	0.70 \pm 0.52	0.23 \pm 0.16	0.08 \pm 0.04
small intestine	2.26 \pm 1.27	1.35 \pm 0.19	0.69 \pm 0.20	0.14 \pm 0.05
large intestine	0.57 \pm 0.15	0.29 \pm 0.06	0.81 \pm 0.51	1.31 \pm 0.9
bladder	1.72 \pm 0.86	7.70 \pm 0.30	1.22 \pm 0.33	1.11 \pm 0.56
PC-3 PIP	28.31 \pm 4.38	28.05 \pm 2.04	26.29 \pm 7.45	23.22 \pm 6.02
PC-3 flu	0.50 \pm 0.07	0.24 \pm 0.06	0.19 \pm 0.08	0.07 \pm 0.01
PIP: flu	53.95 \pm 1.61	112.59 \pm 30.47	103.90 \pm 32.36	307.24 \pm 25.25
PIP: blood	32.14 \pm 4.75	41.24 \pm 26.57	108.72 \pm 28.78	178.00 \pm 79.79
PIP: muscle	42.87 \pm 29.34	38.44 \pm 17.81	103.99 \pm 57.00	141.58 \pm 88.36

^aValues expressed are in % ID/g \pm standard deviation. *N* = 4 for all tissues.

Table 3. Biodistribution of [^{99m}Tc]L11 in Tumor-Bearing Mice^a

	30 min	1 h	2 h	5 h
blood	1.09 ± 0.04	0.47 ± 0.03	0.30 ± 0.03	0.45 ± 0.34
heart	2.34 ± 0.29	1.90 ± 1.28	1.31 ± 0.68	0.61 ± 0.28
lung	7.05 ± 0.95	7.53 ± 0.40	4.54 ± 3.31	3.39 ± 1.94
liver	1.73 ± 0.13	1.25 ± 0.24	0.81 ± 0.08	0.64 ± 0.37
stomach	1.68 ± 0.32	1.62 ± 0.27	0.93 ± 0.18	0.66 ± 0.06
pancreas	3.83 ± 0.45	2.97 ± 1.05	2.82 ± 0.64	1.61 ± 0.21
spleen	88.02 ± 22.76	97.78 ± 29.74	77.57 ± 26.42	45.45 ± 25.43
fat	3.45 ± 0.54	2.65 ± 1.04	0.65 ± 1.31	1.09 ± 1.26
kidney	139.49 ± 12.80	160.90 ± 31.40	159.18 ± 19.50	162.26 ± 11.25
lymph node	8.55 ± 0.84	8.69 ± 4.24	21.52 ± 17.08	33.68 ± 13.01
muscle	1.79 ± 0.30	2.32 ± 1.45	1.18 ± 0.50	0.38 ± 0.33
small intestine	1.53 ± 0.40	2.33 ± 2.49	0.80 ± 0.36	0.44 ± 0.18
large intestine	1.54 ± 0.25	1.04 ± 0.33	0.51 ± 0.34	0.73 ± 0.43
bladder	5.21 ± 1.98	3.14 ± 2.34	2.22 ± 0.63	1.35 ± 0.56
PC3 PIP	35.30 ± 7.04	42.46 ± 4.37	33.59 ± 3.83	30.00 ± 9.60
PC3 flu	2.39 ± 0.80	1.41 ± 0.61	0.77 ± 0.22	0.80 ± 0.43
PIP: flu	15.62 ± 4.44	42.85 ± 0.29.35	46.58 ± 15.90	46.04 ± 27.92
PIP: blood	32.55 ± 6.97	54.92 ± 30.48	111.74 ± 10.84	43.13 ± 37.85
PIP: muscle	20.23 ± 5.04	48.60 ± 48.60	33.93 ± 17.74	57.91 ± 48.65

^aValues expressed are in % ID/g ± standard deviation. N = 4 for all tissues.

Table 4. Biodistribution of [^{99m}Tc]L15 in Tumor-Bearing Mice^a

	30 min	1 h	2 h	5 h
blood	0.53 ± 0.15	0.54 ± 0.07	0.24 ± 0.35	0.19 ± 0.25
heart	0.72 ± 0.23	0.72 ± 0.09	0.17 ± 0.11	0.23 ± 0.06
lung	2.83 ± 0.81	2.59 ± 0.80	1.58 ± 0.45	1.80 ± 0.14
liver	0.62 ± 0.23	0.39 ± 0.05	0.26 ± 0.09	0.24 ± 0.07
stomach	1.01 ± 0.83	1.56 ± 0.65	1.40 ± 0.92	0.45 ± 0.23
pancreas	1.23 ± 0.56	2.36 ± 2.43	0.54 ± 0.20	0.55 ± 0.09
spleen	24.05 ± 9.01	25.66 ± 4.99	7.55 ± 2.14	10.10 ± 2.34
fat	0.85 ± 0.60	1.45 ± 0.44	0.10 ± 0.19	0.35 ± 0.61
kidney	242.68 ± 36.55	346.60 ± 28.12	270.08 ± 44.35	261.65 ± 26.90
muscle	0.83 ± 0.54	0.86 ± 0.02	0.13 ± 0.31	0.34 ± 0.12
sml. intestine	0.46 ± 0.07	0.53 ± 0.36	0.20 ± 0.18	0.38 ± 0.18
lrg intestine	0.48 ± 0.04	0.47 ± 0.21	0.06 ± 0.12	0.25 ± 0.05
bladder	1.09 ± 0.43	1.24 ± 0.86	0.25 ± 0.47	2.42 ± 1.41
PC3 PIP	20.52 ± 2.12	23.44 ± 3.82	18.27 ± 3.35	28.01 ± 5.81
PC3 flu	0.41 ± 0.06	0.43 ± 0.09	0.29 ± 0.13	0.38 ± 0.19
PIP: flu	48.18 ± 7.67	57.40 ± 7.12	70.14 ± 24.93	92.48 ± 40.51
PIP: blood	42.49 ± 21.24	42.57 ± 11.64	67.0328 ± 0.00	63.08 ± 19.84
PIP: muscle	63.69 ± 80.92	18.65 ± 16.57	73.65 ± 0.00	85.42 ± 27.06

^aValues expressed are in % ID/g ± standard deviation. N = 4 for all tissues.

Compounds [^{99m}Tc]L14 and [^{99m}Tc]L15 exhibited high radiotracer concentration both within PSMA+ tumor and kidneys, similar to the distribution profile observed with [^{99m}Tc]L11. Similarly, [^{99m}Tc]L17 and [^{99m}Tc]L18 also demonstrated similar distribution profiles to [^{99m}Tc]L11 at 2 h postinjection. However, faster clearance from kidney than from PSMA+ tumor was noted with [^{99m}Tc]L18 at 18 h postinjection (Supporting Information Figure S6). SPECT-CT images of [^{99m}Tc]L19 demonstrated no specific uptake in PSMA+ tumor or kidneys (Supporting Information Figure S7) and provided diffuse and indiscriminant uptake throughout the tissues.

Biodistribution. On the basis of the SPECT-CT imaging results, [^{99m}Tc]L8, [^{99m}Tc]L11, and [^{99m}Tc]L15 were further assessed in a biodistribution assay using the same PSMA+ PC3 PIP and PSMA- PC3 flu tumor models.²² Tables 2–4 show

the % ID/g uptake values in selected organs for these compounds at 30 min, 1 h, 2 h, and 5 h postinjection. All compounds showed clear PSMA-dependent binding in PSMA+ PC3 PIP tumor xenografts, with [^{99m}Tc]L8, [^{99m}Tc]L11, and [^{99m}Tc]L15 demonstrating high tumor uptake as early as 30 min postinjection and retention of radioactivity at this level up to 5 h postinjection. For [^{99m}Tc]L8, highest tumor uptake was observed at 30 min (28.3 ± 4.4% ID/g). PSMA+ PC3 PIP to PSMA- PC3 flu tumor uptake ratios were 53.9 ± 1.6 and 307.2 ± 24.2 at 30 min and 5 h, respectively. The distribution within normal organs and tissues was also favorable, with low blood and nonspecific tissue uptake and rapid clearance. The highest nonspecific uptake observed was in the liver, 28.9 ± 17.9% ID/g, and spleen, 21.1 ± 8.5% ID/g at 30 min postinjection. However, those values decreased to 3.2 ± 0.4% and 1.8 ± 1.5%, respectively, by 5 h. Kidney uptake was expectedly high and

Table 5. Biodistribution of [for ^{99m}Tc]L11, ^{99m}Tc]L13, ^{99m}Tc]L14, ^{99m}Tc]L15, and ^{99m}Tc]L18 at 2 h Post-Injection in Tumor-Bearing Mice^a

	^{99m}Tc]L11	^{99m}Tc]L13	^{99m}Tc]L14	^{99m}Tc]L15	^{99m}Tc]L18
blood	0.42 ± 0.08	0.35 ± 0.18	0.18 ± 0.04	0.24 ± 0.04	0.49 ± 0.06
heart	2.26 ± 0.64	1.36 ± 0.94	1.62 ± 0.60	1.02 ± 0.41	0.63 ± 0.25
lung	6.68 ± 1.27	4.14 ± 1.91	6.06 ± 0.44	4.43 ± 0.51	3.05 ± 0.94
liver	1.44 ± 0.12	0.80 ± 0.27	1.11 ± 0.13	0.67 ± 0.15	0.76 ± 0.20
stomach	1.10 ± 0.36	0.60 ± 0.15	0.82 ± 0.06	0.82 ± 0.23	0.49 ± 0.19
pancreas	3.45 ± 0.17	1.82 ± 0.64	3.12 ± 0.39	1.66 ± 0.24	1.96 ± 1.20
spleen	47.90 ± 17.12	49.91 ± 21.99	75.29 ± 28.42	45.43 ± 9.82	26.40 ± 8.95
fat	4.82 ± 0.95	2.16 ± 0.83	5.54 ± 3.31	3.60 ± 0.83	4.67 ± 0.01
kidney	134.92 ± 8.61	142.4 ± 12.20	143.42 ± 17.97	226.44 ± 28.03	198.0 ± 34.12
muscle	1.13 ± 0.41	0.94 ± 0.21	1.28 ± 0.43	0.86 ± 0.29	0.43 ± 0.15
sml intest	1.08 ± 0.33	0.97 ± 0.20	0.90 ± 0.30	0.44 ± 0.13	0.42 ± 0.13
lrg intest	0.93 ± 0.43	1.16 ± 0.66	0.84 ± 0.38	0.61 ± 0.07	0.65 ± 0.34
bladder	3.12 ± 0.98	1.66 ± 0.72	2.16 ± 0.73	1.74 ± 0.93	2.61 ± 0.27
PC-3 PIP	26.81 ± 1.94	32.02 ± 15.78	28.67 ± 5.84	24.37 ± 3.12	33.59 ± 3.20
PC-3 flu	0.89 ± 0.09	0.42 ± 0.07	0.69 ± 0.29	0.50 ± 0.12	0.43 ± 0.11
PIP: flu	30.32 ± 2.81	83.12 ± 45.46	46.81 ± 18.49	53.45 ± 17.32	80.14 ± 12.87
PIP: blood	66.99 ± 17.84	92.25 ± 22.53	165.13 ± 53.21	103.40 ± 11.73	69.17 ± 3.94
PIP: muscle	25.70 ± 9.14	48.40 ± 32.08	22.84 ± 11.16	32.88 ± 14.71	82.79 ± 19.99

^aValues expressed are in % ID/g ± standard deviation. N = 4 for all tissues.

peaked at $122.7 \pm 14.7\%$ ID/g at 30 min and decreased to $55.3 \pm 1.2\%$ ID/g by 5 h.

Table 3 shows the organ-related % ID/g of uptake for ^{99m}Tc]L11. Similar to ^{99m}Tc]L8, ^{99m}Tc]L11 showed high PSMA-dependent tumor uptake with $42.5 \pm 4.4\%$ ID/g at 1 h postinjection. Tumor uptake remained high, decreasing to $30.0 \pm 9.6\%$ ID/g at 5 h. The PSMA+ PC3 PIP to PSMA- PC3 flu ratio was 46.6 ± 15.9 at 2 h. Although this is a lower value than that seen for ^{99m}Tc]L8, it is similar to the values observed with one of our original compounds, ^{99m}Tc]L1.¹⁶ The PSMA+ PC3 PIP tumor-to-muscle ratio for ^{99m}Tc]L11 reached a maximum value of 61.7 ± 48.6 at 5 h, about one-half the value for ^{99m}Tc]L8. Renal uptake for ^{99m}Tc]L11 was high at all times and peaked at 5 h at $162.3 \pm 11.3\%$ ID/g, much higher than that seen for ^{99m}Tc]L8. Nontarget organs, such as blood, heart, liver, stomach, and pancreas, showed less uptake ($\sim 2\%$ ID/g at 1 h), which decreased to below 1% ID/g by 5 h. Compound ^{99m}Tc]L11 exhibited high lung uptake ($7.1 \pm 1.0\%$ ID/g at 30 min) compared to ^{99m}Tc]L8, which decreased to $3.4 \pm 1.9\%$ by 5 h. Interestingly, high spleen uptake of $97.8 \pm 30.0\%$ ID/g at 1 h was also observed, which decreased to $45.5 \pm 25.4\%$ ID/g by 5 h.

Table 4 shows the % ID/g of uptake for MAS-3 chelated ^{99m}Tc]L15. Compound ^{99m}Tc]L15, similar to ^{99m}Tc]L8 and ^{99m}Tc]L11, demonstrated PSMA-dependent tumor uptake, which peaked at 5 h at $28.0 \pm 5.8\%$ ID/g. These values are similar to those observed with ^{99m}Tc]L8 but lower than for the MAG-2 conjugated radioligand, ^{99m}Tc]L11. However, PSMA+ PC3 PIP to PSMA- PC3 flu ratios for ^{99m}Tc]L15 were higher than those for ^{99m}Tc]L11, achieving a maximum value of 92.5 ± 40.5 at 5 h. PSMA+ PC3 PIP tumor-to-muscle ratios were also higher, achieving a maximum value of 85.4 ± 27.4 at 5 h as opposed to 48.6 ± 48.6 at 1 h, which was observed for ^{99m}Tc]L11. Nontarget organs, except for spleen, demonstrated little to no uptake ($\leq 1\%$ ID/g throughout the study). Spleen uptake for ^{99m}Tc]L15 was also lower than for ^{99m}Tc]L11, peaking at $25.7 \pm 5.0\%$ ID/g at 1 h, decreasing to $10.1 \pm 2.3\%$ ID/g by 5 h postinjection. Kidney uptake for ^{99m}Tc]L15 was significantly

higher than for ^{99m}Tc]L11 at all time points, with a peak value at 1 h postinjection of $347.0 \pm 28.0\%$ ID/g.

^{99m}Tc]L11 and ^{99m}Tc]L15 were also compared to ^{99m}Tc]L13, ^{99m}Tc]L14, and ^{99m}Tc]L18 in a single time point (2 h) biodistribution study (Table 5). Syntheses and biodistributions were performed on the same day as close to one another as possible to minimize the changes in specific activity. The biodistribution and imaging data reveal several important points regarding the in vivo properties of these compounds. First, the MAG-2 conjugated radiotracers ^{99m}Tc]L11 and ^{99m}Tc]L13 showed high levels of uptake in PSMA+ PC3 PIP tumor and kidney, however, with ^{99m}Tc]L11 having slightly higher nonspecific uptake observed in PSMA- PC3 flu tumor and other organs which resulted in overall lower tumor-to-organ ratios than for ^{99m}Tc]L13. However, in the imaging studies, we noted considerable gastrointestinal uptake of ^{99m}Tc]L13, which could not be captured in the limited tissue biodistribution study. Imaging results alone indicate that ^{99m}Tc]L11 demonstrates superior image contrast compared to ^{99m}Tc]L13. Second, between the MAG-2, MAG-3, and MAS-3 conjugated radiotracers, all exhibited similar tumor uptake ($\sim 20\%$ ID/g), however, ^{99m}Tc]L15, which employs a MAS-3 chelator, exhibited ~ 2 -fold higher accumulation of radioactivity within kidneys than did ^{99m}Tc]L11 or ^{99m}Tc]L14, perhaps due to the presence of three polar hydrophilic functional groups on the chelator backbone. Third, between the hydrophilic ^{99m}Tc]L15 (MAS-3) and ^{99m}Tc]L18, the latter, with two carboxylic acid groups from Asp residues on the chelator side chain, showed higher tumor uptake and lower accumulation of radioactivity in most normal tissues, including spleen, resulting in higher tumor-to-organ ratios than for ^{99m}Tc]L15.

To investigate the cause of the high spleen uptake for the ^{99m}Tc -oxo compounds, two blocking studies were performed on selected organs using normal (nontumor) male CD-1 mice as shown in Table 6, employing both 2-(phosphonomethyl)-pentanedioic acid (2-PMPA)³⁰ and ZJ43 for ^{99m}Tc]L15. Greater than 90% of uptake observed could be blocked in

Table 6. Biodistribution of [^{99m}Tc]L15 Using ZJ43 and 2-PMPA as Blocking Agents in Healthy Male CD-1 Mice at 2 h Postinjection^a

	[^{99m} Tc]L15	[^{99m} Tc]L15 + ZJ43	[^{99m} Tc]L15 + 2-PMPA
blood	0.27 ± 0.02	0.21 ± 0.02	0.22 ± 0.02
spleen	6.34 ± 2.01	0.14 ± 0.05	0.10 ± 0.01
kidney	105.21 ± 10.92	1.54 ± 0.20	1.69 ± 0.72
muscle	0.49 ± 0.17	0.51 ± 0.54	0.34 ± 0.02
testis	0.82 ± 0.10	0.09 ± 0.01	0.14 ± 0.08

^aValues expressed are in % ID/g ± standard deviation. N = 4 for all tissues.

spleen, testis, and kidney, suggesting that the uptake in these tissues is PSMA-mediated.

DISCUSSION

Previously, we reported ^{99m}Tc-labeled PSMA inhibitors with an optimized linker length and obtained a high-affinity radioligand, [^{99m}Tc]L1 (Figure 1), using the single amino acid chelating agent (SAAC) to incorporate ^{99m}Tc.^{16,31} Utilizing the same linker construct, we have now synthesized and evaluated 12 new ^{99m}Tc-labeled PSMA-targeting radioligands (Figure 1), which vary primarily with respect to lipophilicity and charge, using well-established ^{99m}Tc labeling techniques.^{32,33} Our previously published compound, [^{99m}Tc]L1, carries a positive charge. To complement [^{99m}Tc]L1 and the rest of our previous series that relied upon SAAC technology, we synthesized three neutral Tc(I)-tricarboxyl labeled radioligands, [^{99m}Tc]L8–L10, and seven negatively charged ^{99m}Tc-oxo labeled complexes, [^{99m}Tc]L11–L16. Of these, [^{99m}Tc]L11–L15 utilize the N₃S chelator. Radiotracers [^{99m}Tc]L11–L13 contain a previously reported, mercaptoacetyl-Gly-Gly (MAG-2) chelating agent along with hydrophobic substituents, such as Phe groups placed on the linker, to investigate pharmacokinetic effects of these modifications.^{34,35} Consistent with that previously described by Liu et al., [^{99m}Tc]L11–L13 and [^{99m}Tc]L16 were obtained as two diastereomers (*syn* and *anti*) due to the relative orientation of the functional group (carboxylate or Phe residue) on the chelator to the Tc=O core. Also, chelating agent mercaptoacetyl-Gly-Gly-Gly (MAG-3) was used to synthesize [^{99m}Tc]L14.³⁴ We envisioned that introduction of hydroxyl groups may improve clearance from nontarget tissues; therefore, we synthesized a more hydrophilic version of this compound, [^{99m}Tc]L15, with the mercaptoacetyl-Ser-Ser-Ser (MAS-3) chelating group, which has three hydroxyl groups. Compound [^{99m}Tc]L16 employed a diamide dithiol (N₂S₂) chelating agent, reported to form stable ^{99m}Tc-oxo complexes.^{35,36} Because compounds [^{99m}Tc]L11–L16 form negatively charged ^{99m}Tc complexes at physiological pH, to investigate the effect of this charge on pharmacokinetics, we synthesized compounds [^{99m}Tc]L17 and [^{99m}Tc]L18, which are reported to form neutral ^{99m}Tc-oxo complexes.³⁷ Compounds [^{99m}Tc]L17 and [^{99m}Tc]L18 use Cys-Asp-Gly and Cys-Asp-Asp chelators, respectively. We also synthesized compound [^{99m}Tc]L19 using the HYNIC core and tricine as a coligand for ^{99m}Tc labeling.³² All of the compounds were equally synthetically accessible and easy to purify and administer. The 12 compounds studied had similar affinities, in the low nanomolar range, similar to the majority of the PSMA-binding imaging agents we have developed to date.^{16,22,25}

The rationale for the use of these different chelators was to exploit the different coordination chemistry of ^{99m}Tc using

different well-established labeling strategies. For example, [^{99m}Tc(CO)₃]⁺-labeled complexes are robust due to their kinetic inertness and do not, in general, dissociate in vivo. However, because of their organometallic nature, these compounds tend to be lipophilic. ^{99m}Tc-oxo compounds, on the other hand, are stable in the circulation but show increased renal retention. As a result, we observed a clear shift in the pharmacokinetics for the tricarbonyl complexes [^{99m}Tc]L8–L10 in terms of liver uptake and the extent of hepatobiliary excretion when compared to the polar ^{99m}Tc-oxo compounds. Elevated renal radioactivity generally observed with ^{99m}Tc-oxo complexes was further compounded by the high level of PSMA expression in murine kidney.³⁸ Changing the chelator also allows manipulation of the overall charge, while molecular weight and lipophilicity of these compounds can be altered with minor modifications in the linker. In agreement with previously published results on chelate stability and in vivo performance of different bioconjugates such as affibodies³⁹ and peptides^{40–42} using same the ^{99m}Tc-labeling core, we observed significant changes in the biodistribution pattern mostly in nonspecific tissue rather than in PSMA-specific tumor uptake.

SPECT imaging revealed that [^{99m}Tc]L8, the most hydrophilic radioligand in the tricarbonyl series, had high and specific tumor uptake in the PSMA+ PC3 PIP tumor and long tumor retention of radioactivity, with nearly 82% of the initial uptake (30 min) retained even at 5 h postinjection. This is a significant improvement over the previous lead compound [^{99m}Tc]L1, where radiotracer was nearly completely cleared from tumor by 5 h postinjection.¹⁶ Compound [^{99m}Tc]L8 showed low uptake in normal tissues such as liver and gallbladder at late time points. Rapid clearance observed from blood suggested that there was no transchelation to blood proteins. Similarly rapid clearance was also observed from liver, spleen, and kidney. Because the tumor models were derived from isogenic human PC3 Pca cells and are relatively uniform in size and location,⁴³ we surmise that the overall neutral charge, small size of the chelating agent, and relative hydrophilicity of L8 contributed to the high and specific binding to PSMA with rapid clearance from normal tissues.

The most striking feature of the ^{99m}Tc-oxo series is the high and prolonged uptake within spleen, which was not observed for radioligands employing the tricarbonyl chelator. We hypothesize that elevated spleen uptake and retention could be related to binding to a homologue of PSMA, namely glutamate carboxypeptidase III (GCPIII), which has recently been described.^{44,45} GCPIII is highly expressed in spleen, testis, and kidney⁴⁶ and has been shown to be a target of some low molecular weight antagonists of PSMA.⁴⁷ Because none of these antagonists are specific for GCPIII, our blocking studies with 2-PMPA, which has demonstrated affinity to GCPIII, and ZJ43 are not conclusive regarding GCPIII-mediated binding. Blocking studies performed for [^{99m}Tc]L15 in blood, spleen, and kidney do indicate GCPII- and/or GCPIII-mediated tissue uptake. However, because blocking was >90% for both compounds, a significantly greater element of blocking for 2-PMPA could not be demonstrated, which may have suggested a GCPIII-specific element. In a recent preclinical study, high spleen and kidney uptake by a ⁶⁸Ga-labeled Lys-Glu urea-based PSMA PET agent using *N,N'*-bis[2-hydroxy-5-(carboxyethyl)-benzyl]ethylenediamine-*N,N'*-diacetic acid (HBED-CC) as the chelating agent has been reported.⁴⁸ However, the first clinical study of this agent demonstrated only moderate uptake within spleen, which did not interfere with detection of putatively

PSMA+ lesions.⁴⁹ These findings suggest that a species-related difference, perhaps due to differential expression of GCPIII, exists and that elevated uptake in some nontarget sites such as spleen in preclinical rodent studies may not apply to clinical studies.

Considerations for clinical translation of one or more of the radioligands studied herein, or other compounds of this class, include: (1) high concentration within tumor (% ID/g), (2) high binding specificity (PSMA+ PC3 PIP to PSMA- PC3 flu uptake ratio), (3) longer retention in PSMA+ PC3 PIP vs kidney, and (4) low liver and gastrointestinal uptake. While difficult to optimize for all of these parameters concurrently, the compounds synthesized in this small series could be ranked with respect to their desirability for translation. Because all 12 ^{99m}Tc-labeled compounds demonstrated high tumor uptake (>20% ID/g at 2 h postinjection), we next compared the values in PSMA+ PC3 PIP to PSMA- PC3 flu tumors. Compound [^{99m}Tc]L8 proved superior in this regard, as well as with respect to PSMA+ PC3 PIP tumor-to-blood, tumor-to-kidney, and tumor-to muscle ratios. Despite high tumor uptake, other compounds had either confounding gastrointestinal or spleen uptake, difficult to predict based on charge and lipophilicity. Overall, [^{99m}Tc]L8 demonstrated characteristics most consistent with a clinically viable agent among both the tricarbonyl and ^{99m}Tc-oxo species.

CONCLUSIONS

We have synthesized 12 new low-molecular-weight, urea-based, ^{99m}Tc-labeled, PSMA-targeted radiotracers, which differ in the chelating agent and, in some cases, in lipophilicity by manipulation of the linker moiety. We found that except for HYNIC-labeled [^{99m}Tc]L19, all radioligands demonstrated high tumor uptake and retention with the choice of chelator having a profound effect on pharmacokinetics. Compound [^{99m}Tc]L8 demonstrated improved tumor uptake and bio-distribution characteristics compared to all the newly synthesized and previously reported ^{99m}Tc agents from our laboratory and is likely the most suitable for clinical development. These results indicate that consideration of the chelating agent is critical and must be carefully considered when beginning a new campaign to find the most clinically viable ^{99m}Tc-labeled agent, for compounds of this class and likely for those intended for other biomedically important targets.

EXPERIMENTAL SECTION

A detailed description of general experimental methods is included in the Supporting Information. The purity of tested compounds as determined by analytical HPLC with absorbance at 220 nm was >95%.

(3S,7S,22S)-26-(4-(2-Amino-2-carboxyethyl)-1H-1,2,3-triazol-1-yl)-5,13,20-trioxo-4,6,12,21-tetraazahexacosane-1,3,7,22-tetracarboxylic Acid, L8. To a solution of Fmoc-Lys(N₃)-OH (0.25 g, 0.63 mmol in 8 mL of 2/1 *t*-BuOH/H₂O), was added Boc-L-propargylglycine-DCHA (0.25 g, 0.63 mmol in 2 mL of 2/1 *t*-BuOH/H₂O), followed by sodium ascorbate (4.75 mg, 0.024 mmol in 1 mL water) and Cu(OAc)₂·H₂O (2 mg, 0.012 mmol in 1 mL water) and the mixture stirred at room temperature for 12 h under N₂ at 30 °C. Quadrapure-IDA resin (20 mg) was added to the solution and was gently shaken using mechanical shaker at rt for 2 h to remove Cu(II). The solution was filtered through a Celite bed, and the light-yellow filtrate was evaporated to dryness. The solid residue was thus obtained was partitioned between EtOAc and water. The aqueous phases were re-extracted with EtOAc. The organic phases were combined, dried over Na₂SO₄, and evaporated. The crude product was used without

any purification in the next step where the Fmoc group was removed using 20/80 piperidine/DMF solution at rt to produce 1. Compound 1 was purified using C₁₈ liquid chromatography column and a mobile phase consisting of 80/20 H₂O/CH₃CN and lyophilized. Yield: ~45%. To a solution of compound 2 (0.05 g, 0.09 mmol in 250 μL DMF) was added 1 (0.35 g, 0.09 mmol in 50 μL) and was stirred at rt for 2 h. The solution was removed under vacuum. The crude solid residue, L8, was purified by HPLC using a 85/15 water/acetonitrile (0.1% TFA in each) flow rate 4 mL, R_t 10.2 min. ¹H NMR (DMSO-*d*₆) δ: 8.15 (m, 1H, HNCO(Lys-linker)), 8.05 (s, 1H, HC-triazole), 7.75 (m, 1H, HNCO(Lys)), 6.34 (m, 2H, NH(CO)NH), 4.40–3.99 (m, 7H, H₂N-triazole, H₂C–N(triazole), HC(NHCO₂(Glu), HC(NHCO₂(Lys), HC(NH₂)(triazole)), 3.21 (m, 2H, H₂CCH(triazole)), 3.03 (m, 2H, H₂CNH(Lys)), 2.40–2.09 (m, 6H, H₂CCO₂(Glu), H₂CCO₂(linker), H₂CCO₂(linker)), 1.89–1.55 (m, 6H, H₂CCH(Glu), H₂CCH(Lys-linker), H₂CCH(Lys)), 1.55–1.21 (m, 16H, (CH₂)₂ (Lys), (CH₂)₂ (Lys-Linker), (CH₂)₄ (linker)). ¹³C NMR (DMSO-*d*₆) δ: 175.00 (CO₂H), 174.64 (CO₂H), 174.22 (CO₂H), 172.87 (CO₂H), 172.42 (CONH), 170.44 (CONH), 157.77 (NHCONH), 140.88 (C-triazole), 124.04 (C–H, triazole), 52.73 (CH, Glu), 52.24, 52.11 (CH, Lys), (CH, Lys), 51.91 (CHNH₂), 49.59 (CH, NCH₂(triazole)), 44.16 (CH₂NH), 38.75 (CH₂NH, Lys-linker), 35.87 (CH₂CO, linker), 35.48 (CH₂CO, linker), 32.24 (CH₂CH(triazole)), 30.87 (CH₂CO, Glu), 30.35 (CH₂CH, Glu), 29.78, 29.32, 28.96, 28.86, 28.75, 27.97, 26.57, 25.71 (CH₂(linker), (Lys), (Lys-linker)) 23.09, 22.92, 22.66 (CH₂(Lys)), (CH₂(Lys-linker)). ESMS: 743 [M + H]⁺. HRESI⁺-MS: calcd for C₃₁H₅₀N₈O₁₃, 743.3576 [M + H]⁺; found, 743.3570 (found).

(3S,7S)-26-(4-(2-Amino-2-carboxyethyl)-1H-1,2,3-triazol-1-yl)-5,13,20-trioxo-4,6,12,21-tetraazahexacosane-1,3,7,22-tetracarboxylic Acid Tricarbonyl Rhenium(I), ReL8. L8 (0.050g, 0.67 mmol) was dissolved in 2 mL of water. A solution of [Re(CO)₃(H₂O)₃]Br²³ (0.029g, 0.67 mmol in 0.5 mL methanol) was added, and the reaction mixture was refluxed for 4 h. The crude solid, compound ReL8, was purified by HPLC using a gradient HPLC for 40 min, flow rate 8 mL/min, 80/10 water/acetonitrile (0.1% TFA in each) to 70/10 water/acetonitrile (0.1% TFA in each) water flow rate 8 mL, R_t 9.8 min. ¹H NMR (DMSO-*d*₆) δ: 8.24 (m, 1H, HNCO(Lys-linker)), 8.05 (m, 1H, HC-triazole), 7.75 (m, 1H, HNCO(Lys)), 6.34 (m, 2H, NH(CO)NH), 5.96 (m, 1H, H₂N-triazole), 5.25 (m, 1H, H₂N-triazole), 4.45–3.85 (m, 5H, H₂C–N(triazole), HC(NHCO₂(Glu), HC(NHCO₂(Lys), HC(NH₂)(triazole)), 3.25 (m, 1H, H₂CCH(triazole)), 2.98 (m, 3H, H₂CCH(triazole), H₂CNH(Lys)), 2.31–2.01 (m, 6H, H₂CCO₂(Glu), H₂CCO₂(linker), H₂CCO₂(linker)), 2.01–1.54 (m, 6H, H₂CCH(Glu), H₂CCH(Lys-linker), H₂CCH(Lys)), 1.54–1.22 (m, 16H, (CH₂)₂ (Lys), (CH₂)₂ (Lys-Linker), (CH₂)₄ (linker)). ESMS: 1013 [M + H]⁺. HRESI⁺-MS: calcd for C₃₄H₅₀N₈O₁₆Re, 1013.2898 [M + H]⁺; found, 1013.28986.

2-[3-(1-Carboxy-5-(7-[1-carboxy-5-(carboxymethyl-pyridin-2-ylmethyl-amino)-pentylcarbonyl]-heptanoylamino)-pentyl)-ureido]-pentanedioic Acid, L9. Compound L9 was prepared following Scheme 2 in a total of six steps as described below. Compound 3 was synthesized using commercially available Fmoc-Lys(Boc)-OH and 4-methoxy-benzylchloride in presence of cesium carbonate in DMF at rt.¹⁶ Selective removal of Boc from 3 was performed using *p*-toluenesulfonic acid.¹⁶ Briefly, a solution of 3 (2 g, 3.40 mmol in 20 mL EtOAc) was cooled to 0–2 °C in an ice bath, and *p*-toluenesulfonic acid monohydrate (0.64 g, 2.60 mmol) in 5 mL of absolute ethanol was added. The cooling bath was removed, and the reaction mixture was allowed to warm to room temperature for 2 h. The reaction mixture was then concentrated to a thick oil under reduced pressure, and the mixture was purified by flash chromatography using 5/95 MeOH/CH₂Cl₂ to afford product 4 as colorless solid in 55% (1.24 g, 1.87 mmol) yield. ESIMS *m/z*: 660 [M]⁺. A solution of 4 (0.66 g, 1 mmol, in 40 mL CH₂Cl₂) was neutralized with TEA (140 μL, 1.5 mmol) and was cooled at 4 °C by ice-bath. A solution of pyridine-2-aldehyde (0.086g, 0.8 mmol) was added slowly to the ice cold solution of 4 for a period of 30 min and was stirred for another 30 min. Then ice-bath was removed and the solution was stirred at rt for 2 h. Sodium triacetoxyborohydride (0.43 g, 2 mmol) was added portionwise to the reaction mixture followed by acetic acid (126 μL, 2

mmol) and left for 16 h. Solvent was removed under vacuum, and the residue was dissolved in dichloromethane and extracted with 3 × 50 mL of water. Organic layer was dried under vacuum and purified via a silica gel column using 4–5% methanol/CH₂Cl₂ as an eluent to obtain compound **5** in ~40%, 0.232 g (0.4 mmol) yield. ESI-MS: 580 [M + 1]⁺. A solution of **5** (0.1 g, 0.17 mmol) in 20 mL DMF was cooled to 4 °C. To this was added *t*-butyl bromoacetate (32 μL, 0.17 mmol), potassium iodide (0.028 g, 0.17 mmol), and diisopropyl ethylamine (30 μL, 0.17 mmol), respectively, and the mixture stirred for 2 h. The ice-bath was removed, and the mixture was stirred for 2 days at rt. The solvent was removed under vacuum, and the residue was dissolved in 50 mL of ethyl acetate and washed with 3 × 50 mL water. The organic layer was concentrated under vacuum and purified via a silica gel column using 20/80–30/70 EtOAc/CH₂Cl₂ as eluent. Thus, **6** was obtained in 33% (0.039 g) yield. Compound **6** was treated with 4 mL 1/1 TFA/CH₂Cl₂ at rt for 2 h to simultaneously remove Boc and *t*-butyl groups. After solvent removal, crude solid was lyophilized and treated with 2 mL of 20/80 piperidine/DMF at rt for 20 min. Solvent was removed under vacuum. The colorless crude material was dissolved in water (20 mL) and extracted with ethyl acetate (3 × 10 mL). Compound **7** was obtained from the water layer in 48% yield. Compound **7** was further purified via C₁₈ solid phase extraction. ¹H NMR (MeOD) for **7**: δ 8.25 (d, 1H), 7.82 (t, 1H), 7.33 (t, 1H), 6.65 (d, 2H), 4.2 (m, 1H), 3.82 (s, 2H), 3.20 (s, 2H), 2.85 (t, 2H), 2.62 (t, 2H), 2.75–2.39 (m, 6H). ESI-MS: 295 [M + 1]⁺. A solution of **2**¹⁶ (0.020 g, 0.034 mmol) in 100 μL of DMF was added to a stirred solution of **5** (0.010 g, 0.034 mmol) in 100 μL DMF at rt followed by the addition of DIEA (0.05 μL, 0.034 mmol). The reaction mixture was left for 3 h at room temperature. The reaction mixture was then concentrated under reduced pressure dissolved in 1 mL of water and purified by HPLC using an isocratic method of 80/20 water (0.1% TFA)/acetonitrile (0.1% TFA) as mobile phase, flow rate 4 mL/min; R_p 14 min. ¹H NMR (DMSO-*d*₆): δ 8.24 (m, 1H, HNCO(Lys-linker)), 7.75 (m, 1H, HNCO(Lys)), 8.32 (t, 1H, Py), 7.85 (m, 2H, Py), 7.33 (t, 1H), 6.31 (m, 2H, NH(CO)NH), 4.32–4.18 (m, 3H, HC(NHCO₂(Glu)), HC(NHCO₂(Lys)), HC(NHCO₂(Lys))), 4.14 (m, 2H, PyCH₂), 3.42 (m, 2H, CH₂CO₂), 2.95 (m, 4H, H₂CNH(Lys), H₂CNH(Lys-linker)), 2.32–2.02 (m, 6H, H₂CCO₂(Glu), H₂CCO₂(linker), H₂CCO₂(linker)), 2.01–1.56 (m, 6H, H₂CCH(Glu), H₂CCH(Lys-linker), H₂CCH(Lys)), 1.55–1.21 (m, 16H, (CH₂)₂ (Lys), (CH₂)₂ (Lys-linker), (CH₂)₄ (linker)). ESIMS *m/z*: 753 [M + H]⁺. HRFAB⁺-MS: calcd for C₃₄H₅₃N₆O₁₃ [M + H]⁺, 753.3671; found, 753.3675.

2-[3-[5-(7-(5-[Bis-(1*H*-imidazol-2-ylmethyl)-amino]-1-carboxy-pentylcarbamoyl)-heptanoylamino)-1-carboxy-pentyl]-ureido]-pentanedioic Acid, L10. The bisimidazolyl lysine chelate, **8**, was prepared following a literature procedure.¹⁶ Briefly, Fmoc-Lys-OH was reacted with imidazole-2 aldehyde in the presence of NaBH(OAc)₃ and acetic acid in dichloroethane. Solution was stirred for 20 h. The product was diluted with CH₂Cl₂ and washed with water. The solid residue obtained after evaporation of the organic layer was further purified by SiO₂ column chromatography using 20/80 MeOH/CH₂Cl₂ as eluant. Fmoc removal of the compound was performed using a 20/80 piperidine/DMF solution. After solvent removal, compound was purified using a C₁₈ solid phase extraction using 90/10 H₂O/CH₃CN as eluant. ESI-MS 307 [M + H]⁺. Compound **8** (10 mg, 0.03 mmol) in 1 mL DMF was added to a solution of **2** (28 mg, 0.06 mmol) and DIEA (50 μL) and left for 2 h at rt. After solvent evaporation, product was purified using a C₁₈ column. The compound was further purified by HPLC using same method as **L8**, R_p 13.5 min. ¹H NMR (DMSO-*d*₆): δ 8.24 (m, 1H, HNCO(Lys-linker)), 7.75 (m, 1H, HNCO(Lys)), 7.21 (ds, 2H, Im), 7.06 (ds, 2H, Im), 6.34 (m, 2H, NH(CO)NH), 4.33–4.10 (m, 7H, ImCH₂, HC(NHCO₂(Glu)), HC(NHCO₂(Lys)), HC(NHCO₂(Lys)), 3.0–2.95 (4H, H₂CNH(Lys), H₂CNH(Lys)), 2.32–2.02 (m, 6H, H₂CCO₂(Glu), H₂CCO₂(linker), H₂CCO₂(linker)), 2.01–1.55 (m, 6H, H₂CCH(Glu), H₂CCH(Lys-linker), H₂CCH(Lys)), 1.55–1.20 (m, 16H, (CH₂)₂ (Lys), (CH₂)₂ (Lys-linker), (CH₂)₄ (linker)). HRESI⁺-MS: calcd for C₃₄H₅₃N₉NaO₁₁, 786.3762 [M + Na]⁺; found, 786.3757(found).

Synthesis of L11–L18. These compounds were prepared following a combined solid phase and solution phase synthetic strategy as described for **L11**.

2-[3-[1-Carboxy-5-(7-(5-carboxy-5-[3-phenyl-2-(3-phenyl-2-[2-[2-(2-tritylsulfanyl-acetyl-amino)-acetyl-amino]-acetyl-amino]-propionyl-amino)-propionyl-amino]-pentylcarbamoyl)-heptanoylamino]-pentyl]-ureido]-pentanedioic Acid, L11. Lys(Boc)-Wang resin (250 mg, 0.43 mmol) was allowed to swell with CH₂Cl₂ (3 mL) followed by DMF (3 mL). A solution of 20% piperidine in DMF (3 × 3 mL) was added to the resin, followed by gently shaking on a mechanical shaker for 30 min at ambient temperature. The resin was washed with DMF (3 × 3 mL) and CH₂Cl₂ (3 × 3 mL). Formation of free amine was assessed by the Kaiser test.⁵⁰ After swelling the resin in DMF, a solution of Fmoc-Gly-OH (3 equiv), HBTU (3 equiv), HOBt (3 equiv), and DIPEA (4.0 equiv) in DMF was added and gently shaken for 2 h. The resin was then washed with DMF (3 × 3 mL). The coupling efficiency was assessed by the Kaiser test. The aforementioned sequence was repeated for two more coupling steps with Fmoc-Gly-OH. Final compound was cleaved from the resin using TFA/CH₂Cl₂/TES (1:1:0.02) and concentrated under vacuum to produce **9**. The concentrated product was purified by using a C₁₈ SepPak Vac 10g column. The product was eluted with a solution 70/30 water/acetonitrile (0.1% TFA in each). ESIMS: 482 [M]⁺. Lyophilized **9** (100 mg, 207 μmol) in 5 mL of DMF was added to **2** (120 mg, 207 μmol) in 4 mL DMF followed by DIEA (428 μmol, 60 μL) and then stirred at rt for 2 h. After solvent removal, the colorless solid residue thus obtained was purified by solid phase extraction by using a C₁₈ SepPak Vac 10g column using an eluent of 60/40 water/acetonitrile (0.1% TFA in each). ESIMS: 941 [M + H]⁺. Yield: ~70 mg, (36%). The isolated compound (70 mg, 74 μmol) was treated with 20/80 piperidine/DMF solution (5 mL × 2) to remove Fmoc group. Some colorless precipitate was appeared. Water (0.1 mL) was added to the reaction mixture to dissolve the precipitate and left at rt for 5 min and was purified by solid phase extraction (C₁₈ SepPak Vac 5g column using an eluent of 85/15 water/acetonitrile (0.1% TFA in each)). ESIMS: 717 [M]⁺. Yield: ~35 mg (~66%). To a solution of NHS-ester of mercaptoacetic acid²⁴ (26 mg, 60 μmol) in 3 mL of DMF was added the above compound (36 mg, 50 μmol) in 2 mL of DMF for 2h at rt. After solvent removal product was purified by preparative RP-HPLC to obtain **L11** in ~20 mg (32%). **L11–L15** purified by same general HPLC method. The solvent system is 0–5 min 60% A and 40% B, 5–25 min 60–50% A and 40–50% B, 25–35 min 50–60% A and 50–40% B, Flow rate 4 mL/min, R_p 11.2 min. ¹H NMR (DMSO-*d*₆): δ 8.23–7.76 (m, 5H, HNCO(Lys-linker), HNCO(Lys), HNCO(Gly)), 7.42–7.20 (m, 15H, trityl), 6.34 (m, 2H, NH(CO)NH), 4.33–3.98 (m, 7H, HC(NHCO₂(Glu)), HC(NHCO₂(Lys)), HC(NHCO₂(Lys)), H₂CNH(Gly)(2)), 3.54 (m, 2H, H₂C-S-trityl), 3.0–2.95 (4H, H₂CNH(Lys), H₂CNH(Lys)), 2.32–2.02 (m, 6H, H₂CCO₂(Glu), H₂CCO₂(linker), H₂CCO₂(linker)), 2.05–1.53 (m, 6H, H₂CCH(Glu), H₂CCH(Lys-linker), H₂CCH(Lys)), 1.53–1.22 (m, 16H, (CH₂)₂ (Lys), (CH₂)₂ (Lys-linker), (CH₂)₄ (linker)). HRESI⁺-MS: calcd for C₅₁H₆₈N₇O₁₄S, 1034.4545 [M + H]⁺; found, 1034.4542.

12-Benzyl-4,7,10,13,21,28,36-heptaooxo-1,1,1-triphenyl-2-thia-5,8,11,14,20,29,35,37-octaazatetracontane-15,34,38,40-tetracarboxylic Acid, L12. MAG-2 chelator, amino acid residues are Lys, Gly, Gly, Phe. R_p 16 min. ¹H NMR (DMSO-*d*₆): δ 8.23–7.76 (m, 6H, HNCO(Lys-linker), HNCO(Lys), HNCO(Gly), HNCOPhe)), 7.42–7.20 (m, 20H, trityl, Ph), 6.34 (m, 2H, NH(CO)NH), 4.33–3.98 (m, 8H, HC(NHCO₂(Glu)), HC(NHCO₂(Lys)), HC(NHCO₂(Lys)), HCNH(Phe), H₂CNH(Gly)(2)), 3.54–3.44 (m, 4H, H₂C-S-trityl, H₂C(Phe)), 3.0–2.95 (4H, H₂CNH(Lys), H₂CNH(Lys)), 2.32–2.06 (m, 6H, H₂CCO₂(Glu), H₂CCO₂(linker), H₂CCO₂(linker)), 2.02–1.55 (m, 6H, H₂CCH(Glu), H₂CCH(Lys-linker), H₂CCH(Lys)), 1.55–1.21 (m, 16H, (CH₂)₂ (Lys), (CH₂)₂ (Lys-linker), (CH₂)₄ (linker)). HRESI⁺-MS: calcd for C₆₀H₇₇N₈O₁₅S, 1180.5151 [M + H]⁺; found, 1180.5154.

12,15-Dibenzyl-4,7,10,13,16,24,31,39-octaooxo-1,1,1-triphenyl-2-thia-5,8,11,14,17,23,32,38,40-nonaazatritetracontane-18,37,41,43-tetracarboxylic Acid, L13. MAG-2 chelator, amino acid residues are Lys, Gly, Gly, Phe, Phe. R_p 22 min. ¹H NMR (DMSO-*d*₆): δ 8.23–

7.76 (m, 7H, HNCO(Lys-linker), HNCO(Lys), HNCO(Gly), HNCOPhe), 7.42–7.20 (m, 25H, trityl, Ph), 6.34 (m, 2H, NH(CO)NH), 4.33–3.98 (m, 9H, HC(NHCO₂(Glu), HC(NHCO₂(Lys), HC(NHCO₂(Lys), HCNH(Phe), H₂CNH(Gly)(2)), 3.54–3.41 (m, 6H, H₂C–S-trityl, H₂C(Phe) (2)), 3.0–2.95 (4H, H₂CNH(Lys), H₂CNH(Lys)), 2.32–2.03 (m, 6H, H₂CCO₂(Glu), H₂CCO₂(linker), H₂CCO₂(linker)), 2.02–1.56 (m, 6H, H₂CCH(Glu), H₂CCH(Lys-linker), H₂CCH(Lys)), 1.55–1.20 (m, 16H, (CH₂)₂ (Lys), (CH₂)₂ (Lys-Linker), (CH₂)₄ (linker)). HRESI⁺-MS: calcd for C₆₉H₈₆N₉O₁₆S, 1328.5913 [M + H]⁺; found, 1328.5917.

4,7,10,13,21,28,36-Heptaaxo-1,1,1-triphenyl-2-thia-5,8,11,14,29,35,37-heptaazatetracontane-15,34,38,40-tetracarboxylic Acid, L14. MAG-3 chelator, amino acid residues are Lys, Gly, Gly, Gly. R_v, 13 min. ¹H NMR (DMSO-*d*₆): δ 8.23–7.76 (m, 6H, HNCO(Lys-linker), HNCO(Lys), HNCO(Gly)), 7.42–7.20 (m, 15H, trityl), 6.34 (m, 2H, NH(CO)NH), 4.33–3.98 (m, 9H, HC(NHCO₂(Glu)), HC(NHCO₂(Lys)), HC(NHCO₂(Lys)), HCNH(Gly)(3)), 3.54 (m, 2H, H₂C–S-trityl), 3.0–2.95 (4H, H₂CNH(Lys), H₂CNH(Lys)), 2.32–2.02 (m, 6H, H₂CCO₂(Glu), H₂CCO₂(linker), H₂CCO₂(linker)), 2.0–1.55 (m, 6H, H₂CCH(Glu), H₂CCH(Lys-linker), H₂CCH(Lys)), 1.54–1.23 (m, 16H, (CH₂)₂ (Lys), (CH₂)₂ (Lys-linker), (CH₂)₄ (linker)). HRESI⁺-MS: calcd for C₅₄H₇₂N₇O₁₅S, 1090.4907 [M + H]⁺; found, 1090.4910.

(19S,34S,38S)-6,9,12-Tris(hydroxymethyl)-4,7,10,13,21,28,36-heptaaxo-1,1,1-triphenyl-2-thia-5,8,11,14,20,29,35,37-octaazatetracontane-19,34,38,40-tetracarboxylic Acid, L15. MAS-3 chelator, amino acid residues are Lys, Ser, Ser, Ser. R_v, 9 min. ¹H NMR (DMSO-*d*₆): δ 8.23–7.76 (m, 6H, HNCO(Lys-linker), HNCO(Lys), HNCO(Ser)), 7.42–7.20 (m, 15H, trityl), 6.34 (m, 2H, NH(CO)NH), 4.63–3.98 (m, 12H, HCNH(Ser)(3), HC(NHCO₂(Glu), HC(NHCO₂(Lys)), HC(NHCO₂(Lys-linker), H₂CCO₂((Ser)(3))), 3.67 (sb, 3H, HOCH₂), 3.54 (m, 2H, H₂C–S-trityl), 3.0–2.95 (4H, H₂CNH(Lys), H₂CNH(Lys)), 2.32–2.03 (m, 6H, H₂CCO₂(Glu), H₂CCO₂(linker), H₂CCO₂(linker)), 2.02–1.56 (m, 6H, H₂CCH(Glu), H₂CCH(Lys-linker), H₂CCH(Lys)), 1.55–1.23 (m, 16H, (CH₂)₂ (Lys), (CH₂)₂ (Lys-linker), (CH₂)₄ (linker)). HRESI⁺-MS: calcd for C₅₅H₇₇N₈O₁₈S₂, 1181.5077 [M + H]⁺; found, 1181.50781.

(10R,29S,33S)-4,8,16,23,31-Pentaaxo-1,1,1-triphenyl-7-(2-(tritylthio)acetamido)-2-thia-5,9,15,24,30,32-hexaazapentatriacontane-10,29,33,35-tetracarboxylic Acid, L16. Diamide dithiol (DADT) chelating agent, amino acid residues are Lys and 1,3-diaminopropionic acid. R_v, 49 min, the HPLC method is 0–10 min 70% A and 30% B, 10–60 min 70–10% A and 30–90% B, 60–65 min 10–70% A and 90–30% B, Flow rate 8 mL/min. ¹H NMR (DMSO-*d*₆): δ 8.25–7.98 (m, 5H, HNCO(Lys-linker), HNCO(Lys), NHCO(Dap)), 7.45–7.14 (m, 30H, trityl), 6.37–6.33 (m, 2H, NHCONH), 5.10 (m, 1H, CHNH, dap), 4.33–4.20 (m, 3H, HC(NHCO₂(Glu), HC(NHCO₂(Lys)), HC(NHCO₂(Lys-linker)), 3.54–3.34 (m, 6H, H₂C–S-trityl, H₂CNH₂(dap)), 3.02–2.99 (m, 4H, H₂CNH(Lys), H₂CNH(Lys)), 2.27–2.20 (m, 2H, H₂CCH(Glu)), 2.20–2.00 (m, 4H, H₂CCH(Lys-linker), H₂CCH(Lys)), 1.92–1.62 (m, 6H, H₂CCH(Glu), H₂CCH(Lys-linker)), 1.52–1.26 (m, 16H, (CH₂)₂ (Lys), (CH₂)₂ (Lys-linker), (CH₂)₄ (linker)). HRESI⁺-MS: calcd for C₇₁H₈₄N₇O₁₄S₂, 1322.5518 [M + H]⁺; found, 1322.5520.

2-(3-(19-1-Carboxy-pentylcarbamoil)-heptanoylamino]-1-carboxy-pentyl]-ureido)-pentanedioic Acid, L17. Amino acid residues are Lys, Cys, Asp, Gly. R_v, 38 min. Compound **12** (10 mg, 15.5 μmol in 0.5 mL) was mixed with **2** (10 mg, 7.4 μmol, 17.4 in 1 mL DMF) and left at rt for 2 h. Solvent was reduced under vacuum, and residue showed the expected mass 1100 [M + H]⁺. The residue was dissolved in 1 mL of 20/80 piperidine/DMF. Some colorless precipitate was appeared. Water (0.1 mL) was added to the reaction mixture to dissolve the precipitate and left at rt for 5 min. The solution was evaporated to dryness, and the residue was dissolved in water and purified by HPLC to isolate **L17** using the same method as **L16**. R_v, 20 min. ¹H NMR (DMSO-*d*₆): δ 8.22–7.86 (m, 5H, HNCO(Lys-linker), HNCO(Lys), NHCO(Cys) NHCO (Asp)), 6.35–6.30 (m, 2H, NHCONH), 4.81–3.89 (m, 5H, HCNH(Cys), HCNH(Asp), HC(NHCO₂(Glu), HC(NHCO₂(Lys)), HC(NHCO₂(Lys-linker)), 3.65–3.02 (m, 6H, H₂CNH₂(Gly), H₂CSH, H₂CCO₂ (Asp)), 3.02–

2.99 (m, 4H, H₂CNH(Lys), H₂CNH(Lys)), 2.27–2.20 (m, 2H, H₂CCH(Glu)), 2.20–2.00 (m, 4H, m, 4H, H₂CCO₂(linker), H₂CCO₂(linker)), 1.92–1.62 (m, 6H, H₂CCH(Glu), H₂CCH(Lys-linker)), 1.52–1.26 (m, 16H, (CH₂)₂ (Lys), (CH₂)₂ (Lys-linker), (CH₂)₄ (linker)). ESIMS 878 [M]⁺. HRESI⁺-MS: calcd for C₃₅H₅₉N₈O₁₆S, 879.3770; found, 879.3770.

5-Amino-32-(carboxymethyl)-29-(mercaptomethyl)-5,13,20,28,31,34-hexaaxo-4,6,12,21,27,30,33-heptaazahexatriacontane-1,3,7,26,36-pentacarboxylic Acid, L18. Amino acid residues are Lys, Cys, Asp, Asp. R_v, 18 min, (HPLC method same as **L16**) 8.23–7.97 (m, 5H, HNCO(Lys-linker), HNCO(Lys), NHCO(Cys) NHCO (Asp)), 6.35–6.30 (m, 2H, NHCONH), 4.81–3.89 (m, 6H, HCNH(Cys), HCNH(Asp), HC(NHCO₂(Glu), HC(NHCO₂(Lys)), HC(NHCO₂(Lys-linker))), 3.65–3.02 (m, 6H, H₂CSH, H₂CCO₂ (Asp)), 3.02–2.99 (m, 4H, H₂CNH(Lys), H₂CNH(Lys)), 2.27–2.20 (m, 2H, H₂CCH(Glu)), 2.20–2.00 (m, 4H, H₂CCO₂(linker), H₂CCO₂(linker)), 1.92–1.62 (m, 6H, H₂CCH(Glu), H₂CCH(Lys-linker)), 1.53–1.26 (m, 16H, (CH₂)₂ (Lys), (CH₂)₂ (Lys-Linker), (CH₂)₄ (linker)). HRESI⁺-MS: calcd for C₃₇H₆₀N₈O₁₈S, 936.3746 [M]⁺; found, 936.3748.

2-(3-[1-Carboxy-5-(7-(1-carboxy-5-[(6-hydrazino-pyridine-3-carbonyl)-amino]-pentylcarbamoil)-heptanoylamino]-pentyl]-ureido)-pentanedioic Acid, L19. To a solution of **10**²⁵ (10 mg, 16 μmol, 0.5 mL DMSO) was added HYNIC-OSu (12 mg, 32 μmol in 0.5 mL DMSO) and DIEA (50 μL) and left at rt for 2 hr. After solvent evaporation, the compound was purified using 2g C₁₈ cartridge. The product was lyophilized. Compound was treated 1/1 of 2 mL of TFA/CH₂Cl₂ for 2 h at rt. After solvent evaporation, the solid residue was purified by HPLC (method same as **L8**), R_v, 12.5 min. ¹H NMR (DMSO-*d*₆): 8.35 (s, 1H, Py), 8.23 (m, 1H, HNCO(Lys-linker)), 7.75 (m, 2H, HNCO(Lys), CHPy), 7.25 (m, 1H, CHPy), 6.35–6.30 (m, 2H, NHCONH), 4.13–3.92 (m, 3H, HC(NHCO₂(Glu), HC(NHCO₂(Lys), HC(NHCO₂(Lys-linker))), 3.01–2.98 (m, 2H, H₂CNH(Lys)), 2.27–2.20 (m, 2H, H₂CCO₂(Glu)), 2.22–2.02 (m, 4H, H₂CCO₂(linker), H₂CCO₂(linker)), 2.09–1.65 (m, 6H, H₂CCH(Glu), H₂CCH(Lys-linker), 1.52–1.23 (m, 16H, (CH₂)₂ (Lys), (CH₂)₂ (Lys-Linker), (CH₂)₄ (linker)). HRESI⁺-MS: calcd for C₃₂H₅₀N₈O₁₂, 738.3548 [M + H]⁺; found, 738.3543(found).

Radiochemistry. All radiolabeled compounds were purified by HPLC using a Phenomenex C₁₈ Luna 10 × 250 mm² 10 μm column. HPLC was performed on a Varian Prostar system (Palo Alto, CA), equipped with a Varian Prostar 325 variable wavelength UV detector and a Bioscan Flow-Count in-line HPLC radioactivity detector. All final compounds were obtained in >98% purity, as determined by HPLC (Supporting Information). The following HPLC solvent methods were used to purify the radiolabeled ligands [^{99m}Tc]**L8**–**L19** from the unlabeled ligand. HPLC was performed using solvent A (0.1% TFA in water) and solvent B (0.1% TFA in CH₃CN), flow rate 4 mL/min. Method 1: gradient method, 0–15 min 90–80% A and 10–20% B, 15–35 min 80–65% A and 20–35% B, 35–45 min 65–90% A and 35–10% B. Method 2: isocratic method, the mobile phase was 80% solvent A and 20% solvent B. Method 3: gradient method, 0–5 min 85% A and 15% B, 5–25 min 85–50% A and 15–50% B, 25–35 min 50–20% A and 50–80% B, 35–40 min 20–85% A and 80–15% B. Method 4: gradient method, 0–5 min 80% A and 20% B, 5–25 min 80–40% A and 20–60% B, 25–35 min 40–80% A and 60–20% B. Method 5: isocratic method, 86% solvent A and 14% solvent B. Retention time of the compounds are listed in Supporting Information Table S1. HPLC chromatograms of [^{99m}Tc]**L8**–**L19** and stability studies of [^{99m}Tc]**L8** and [^{99m}Tc]**L15** are reported in the Supporting Information.

Radiolabeling of L8–L10. These compounds were synthesized in radioactive (^{99m}Tc-labeled) form using the same general method as described previously by us using the Isolink kit.¹⁶ All ^{99m}Tc-labeled compounds were synthesized in radiochemical yields of 60–90% and radiochemical purities of >98%. Briefly, 414.7 MBq (11.2 mCi) in 1 mL of saline Na[^{99m}TcO₄] was added to the Isolink kit, and the reaction mixture was heated in a water bath at 95 °C for 20 min then allowed to cool to rt to prepare [^{99m}Tc(CO)₃(H₂O)₃]⁺. Briefly, for ^{99m}Tc[**L8**] preparation, 500 μL of the [^{99m}Tc(CO)₃(H₂O)₃]⁺ solution

(222 MBq/6 mCi) was neutralized with 100 μL of 1(N) HCl. To this solution was added a 100 μL of phosphate-buffered saline (PBS) solution and 100 μL of a solution of L8 (2 mg, 2.7 μmol in 1 mL water) and was heated at 95 $^{\circ}\text{C}$ for 30 min. This was diluted with 750 μL of the HPLC mobile phase and purified by radio-HPLC. The major radioactive peak constituting desired product (148 MBq/4 mCi) eluted at 28 min. Radiochemical yield: 64.5%. Radiochemical purity > 98%, specific activity > 411 GBq/ μmol (1.1×10^4 mCi/ μmol). For [$^{99\text{m}}\text{Tc}$]L8 and [$^{99\text{m}}\text{Tc}$]L10, method 1 was used. Method 2 was employed to purify [$^{99\text{m}}\text{Tc}$]L9.

Radiolabeling of L11–L18. Radiolabeling for ligands L11–L18 were performed following a literature procedure.²⁶ Briefly, compound L11 (1 mg, 75.3 μmol) was dissolved in 1 mL of 0.5 M ammonium acetate buffer at pH 8. Disodium tartrate dihydrate was dissolved in the labeling buffer of 0.5 M ammonium acetate (pH 8.5) to a concentration of 50 mg/mL. Ascorbic acid–HCl solution was prepared by dissolving ascorbic acid in 10 mM HCl to a concentration of 3.0 mg/mL. A fresh 4 mg/mL SnCl_2 was prepared using ascorbic–HCl solution. A solution of L11 (80 μL) was combined to a solution of 50 μL of 0.25 M ammonium acetate and 20 μL of tartrate buffer. This solution was purged with N_2 for 2 min. To this solution was added the SnCl_2 solution (10 μL), and pH of the solution was adjusted ~ 8 – 8.5 . $^{99\text{m}}\text{Tc}$ -pertechnetate 10–20 mCi in 200 μL was added to the solution and was heated ~ 90 – 100 $^{\circ}\text{C}$ (boiling water bath) for 20 min. Reaction mixture was cooled, diluted with 850 μL of water, and purified by HPLC method 3. Two radiolabeled products were isolated for L11–L13 and designated as [$^{99\text{m}}\text{Tc}$]L11A–L13A (45%) and [$^{99\text{m}}\text{Tc}$]L11B–L13B (55%) with an overall yield ~ 70 – 90% without decay correction. To get a good separation between two radiolabeled products for [$^{99\text{m}}\text{Tc}$]L11–L13A and B, method 4 was used.

Radiolabeling of L19. Tricine was used as coligand for HYNIC labeling. Radiolabeling for ligands L19 was performed following a literature procedure.⁵¹ Briefly, to 50 μL of HYNIC ligand (2 mg/mL) was added 50 μL of 0.5 M NaHCO_3 and 100 μL of tricine (7 mg/mL in water), and the solution was purged with N_2 for 2 min. $\text{Na}^{99\text{m}}\text{TcO}_4$ (185 mBq/5 mCi in 200 μL saline) and 10 μL of freshly prepared SnCl_2 (1 mg/mL in 10 mM HCl) were added to the solution and left at rt for 30 min. HPLC method 5 was used to isolate [$^{99\text{m}}\text{Tc}$]L19. Radiolabeled product was obtained in $\sim 60\%$ yield and $\sim 95\%$ purity.

Formulation. All radiolabeled products were neutralized with ~ 20 – 30 μL of 1 M sodium bicarbonate and evaporated to dryness under vacuum. The obtained solid residues were dissolved in 200 μL of saline and used for imaging and biodistribution studies after appropriate dilution with saline.

Cell Lines. Sublines of the androgen independent PC3 human PCa cell line, originally derived from an advanced androgen independent bone metastasis, were used. These sublines have been modified to express high (PC3 PIP) or possess low (PC3 flu) levels of PSMA and were generously provided by Dr. Warren Heston (Cleveland Clinic). PSMA-expressing (PC3 PIP), nonexpressing (PC3 flu) PCa cell lines were grown in RPMI 1640 medium (Corning Cellgro, Manassas, VA) containing 10% fetal bovine serum (FBS) (Sigma-Aldrich, St. Louis, MO) and 1% penicillin–streptomycin (Corning Cellgro, Manassas, VA). All cell cultures were maintained in an atmosphere containing 5% carbon dioxide (CO_2) at 37.0 $^{\circ}\text{C}$ in a humidified incubator.

NAALADase Assay. The PSMA inhibitory activity of L8–L19 and ReL8 were determined using a fluorescence-based assay according to a previously reported procedure.²² Briefly, lysates of LNCaP cell extracts (25 μL) were incubated with the inhibitor (12.5 μL) in the presence of 4 μM *N*-acetylaspartylglutamate (NAAG) (12.5 μL) for 120 min. The amount of the glutamate released by NAAG hydrolysis was measured by incubating with a working solution (50 μL) of the Amplex Red Glutamic Acid Kit (Life Technologies, Grand Island, NY) for 60 min. Fluorescence was measured with a VICTOR3 V multilabel plate reader (Perkin-Elmer Inc., Waltham, MA) with excitation at 490 nm and emission at 642 nm. Inhibition curves were determined using semilog plots, and IC_{50} values were determined at the concentration at which enzyme activity was inhibited by 50%. Enzyme inhibitory constants (K_i values) were generated using the Cheng–Prusoff conversion.⁵² Assays were performed in triplicate. Data analysis was performed using

GraphPad Prism version 4.00 for Windows (GraphPad Software, San Diego, California).

Tumor Models. Animal studies were carried out in full compliance with the regulations of the Johns Hopkins Animal Care and Use Committee. The 6–8-week-old male, nonobese diabetic (NOD)/severe-combined immunodeficient (SCID) mice (Johns Hopkins Immune Compromised Core) were implanted subcutaneously (sc) with PC3 PIP (PSMA+) and PC3 flu (PSMA–) cells (2×10^6 in 100 μL of HBSS (Corning Cellgro, Manassas, VA) at the forward right and left flanks, respectively. Mice were imaged or used in ex vivo biodistribution assays when the xenografts reached 5–7 mm in diameter.

SPECT-CT Imaging of PSMA+ PC3 PIP and PSMA– PC3 flu Xenografts. Compounds [$^{99\text{m}}\text{Tc}$]L8–L19 were imaged in PSMA+ PC3 PIP and PSMA– PC3 Flu xenograft models. Mice ($N = 2$) were injected via the tail vein with approximately 37 MBq (1 mCi) of radiotracer formulated in 100 μL of saline at pH ~ 7 . Mice were anesthetized with 3% isoflurane, placed in the scanner, and maintained at 1% isoflurane throughout the imaging procedure. A Gamma Medica-Ideas (Northridge, CA) X-SPECT scanner equipped with two opposing low-energy 0.5 mm aperture pinholes and tunable CT was used for all scans. Mice were scanned over 180 $^{\circ}$ in 5.5 $^{\circ}$, 30 s increments. A CT scan was performed prior to or after scintigraphy for anatomical coregistration. Data were reconstructed and fused using commercial software from the vendor (Gamma Medica-Ideas), which includes a 2D-ordered subsets-expectation maximum (OS-EM) algorithm. Volume rendered images were generated using Amira software (<http://www.vsg3d.com/amira>).

In Vivo Binding Specificity. To validate further the specificity of compounds in vivo, mice bearing PSMA+ PC3 PIP and PSMA– PC3 flu tumors were treated with 1 mg of the high-affinity PSMA inhibitor, 2*N*-[[[(1*S*)-1-carboxy-3-methylbutyl]amino]carbonyl]-*L*-glutamic acid, (ZJ43), in 100 μL of saline 30 min prior to the injection of [$^{99\text{m}}\text{Tc}$]L11, ~ 37 MBq (1 mCi in 100 μL of saline).²⁸ SPECT-CT imaging commenced at 30 min after administration of ZJ43, the PSMA blocking agent.

Biodistribution. Mice bearing PSMA+ PC3 PIP and PSMA– PC3 flu xenografts were injected via the tail vein with 1.85 MBq (50 μCi) of [$^{99\text{m}}\text{Tc}$]L8, [$^{99\text{m}}\text{Tc}$]L11, [$^{99\text{m}}\text{Tc}$]L13–L15, or [$^{99\text{m}}\text{Tc}$]L18 ($N = 4$ per study). At 30 min and 1, 2, and 5 h postinjection, mice were sacrificed after which heart, lungs, liver, stomach, pancreas, spleen, fat, kidney, muscle, small and large intestines, urinary bladder, PSMA+ PC3 PIP and PSMA– PC3 flu tumors, and a 0.1–0.2 mL aliquot of blood were collected. Each organ was weighed, and the tissue radioactivity was measured with an automated gamma counter (1282 Compugamma CS, Pharmacia/LKB Nuclear, Inc., Gaithersburg, MD). The percentage of injected dose per gram of tissue (% ID/g) was calculated by comparison with samples of a standard dilution of the initial dose. All measurements were corrected for decay.

Data Analysis. Data are expressed as mean \pm standard deviation (SD). Prism software (GraphPAD, San Diego, California) was used to determine statistical significance. Statistical significance was calculated using a paired *t* test. A *P*-value <0.0001 was considered significant.

■ ASSOCIATED CONTENT

📄 Supporting Information

Detailed general experimental methods, spectral data and supporting SPECT-CT imaging figures. This material is available free of charge via the Internet at <http://pubs.acs.org>.

■ AUTHOR INFORMATION

Corresponding Author

*For S.R.B.: phone, 410-955-8697; fax, 410-614-3147; E-mail, sray9@jhmi.edu; address, Johns Hopkins Medical Institutions, 1550 Orleans Street, 4M07 CRB II, Baltimore, MD 21287. For M.G.P.: phone, 410-955-2789; fax, 443-817-0990; E-mail, mpomper@jhmi.edu; address, Johns Hopkins Medical Institutions, 1550 Orleans Street, 492 CRB II Baltimore, MD 21287.

Notes

The authors declare no competing financial interest.

ACKNOWLEDGMENTS

We are grateful for the following sources of support: K25 CA148901, NIH NCI U54CA151838, NCI CA134675. There are no potential conflicts of interest.

ABBREVIATIONS USED

PSMA, prostate-specific membrane antigen; GCPII, glutamate carboxypeptidase II; NAALADase, N-acetylated- α -linked acid dipeptidase; DCFBC, N-[N-[(S)-1,3-dicarboxypropyl]-carbamoyl]-(S)-4-fluorobenzyl-L-cysteine; PET, positron emission tomography; SPECT, single photon emission computed tomography; SAAC, single amino acid chelate; 2-PMPA, 2-(phosphonomethyl)pentanedioic acid; MAG-2, mercaptoacetyldiglycine; MAG-3, mercaptoacetyltriglycine; MAS-3, mercaptoacetyltriserine; DADT, diamidodithiol and; HYNIC, 2-hydrazinonicotinic acid

REFERENCES

- (1) Pillai, M. R. A.; Dash, A.; Knapp, F. F. Sustained Availability of ^{99m}Tc : Possible Paths Forward. *J. Nucl. Med.* **2013**, *54*, 313–323.
- (2) Alberto, R. *Tc-99m Radiopharmaceuticals: Status and Trends*; Radioisotopes and Radiopharmaceutical Series no. 1; International Atomic Energy Agency: Vienna, 2009.
- (3) Ghosh, A.; Heston, W. D. Tumor Target Prostate Specific Membrane Antigen (PSMA) and its Regulation in Prostate Cancer. *J. Cell Biochem.* **2004**, *91*, 528–539.
- (4) Akhtar, N. H.; Pail, O.; Saran, A.; Tyrell, L.; Tagawa, S. T. Prostate-Specific Membrane Antigen-Based Therapeutics. *Adv. Urol.* **2012**, *2012*, 1–9.
- (5) Chang, S. S.; Reuter, V. E.; Heston, W. D.; Gaudin, P. B. Comparison of Anti-Prostate-Specific Membrane Antigen Antibodies and Other Immunomarkers in Metastatic Prostate Carcinoma. *Urology* **2001**, *57*, 1179–1183.
- (6) Bander, N. H.; Milowsky, M. I.; Nanus, D. M.; Kostakoglu, L.; Vallabhajosula, S.; Goldsmith, S. J. Phase I Trial of ^{177}Lu -Labeled J591, a Monoclonal Antibody to Prostate-Specific Membrane Antigen, in Patients with Androgen-Independent Prostate Cancer. *J. Clin. Oncol.* **2005**, *23*, 4591–4601.
- (7) Perner, S.; Hofer, M. D.; Kim, R.; Shah, R. B.; Li, H.; Moller, P.; Hautmann, R. E.; Gschwend, J. E.; Kuefer, R.; Rubin, M. A. Prostate-Specific Membrane Antigen Expression as a Predictor of Prostate Cancer Progression. *Hum. Pathol.* **2007**, *38*, 696–701.
- (8) Hillier, S. M.; Maresca, K. P.; Femia, F. J.; Marquis, J. C.; Foss, C. A.; Nguyen, N.; Zimmerman, C. N.; Barrett, J. A.; Eckelman, W. C.; Pomper, M. G.; Joyal, J. L.; Babich, J. W. Preclinical Evaluation of Novel Glutamate-Urea-Lysine Analogues that Target Prostate-Specific Membrane Antigen as Molecular Imaging Pharmaceuticals for Prostate Cancer. *Cancer Res.* **2009**, *69*, 6932–6940.
- (9) Foss, C. A.; Mease, R. C.; Cho, S. Y.; Kim, H. J.; Pomper, M. G. GCPII Imaging and Cancer. *Curr. Med. Chem.* **2012**, *19*, 1346–1359.
- (10) Cho, S. Y.; Gage, K. L.; Mease, R. C.; Senthambichelvan, S.; Holt, D. P.; Jeffrey-Kwanisai, A.; Endres, C. J.; Dannals, R. F.; Sgouros, G.; Lodge, M.; Eisenberger, M. A.; Rodriguez, R.; Carducci, M. A.; Rojas, C.; Slusher, B. S.; Kozikowski, A. P.; Pomper, M. G. Biodistribution, Tumor Detection, and Radiation Dosimetry of ^{18}F -DCFBC, a Low-Molecular-Weight Inhibitor of Prostate-Specific Membrane Antigen, in Patients with Metastatic Prostate Cancer. *J. Nucl. Med.* **2012**, *53*, 1883–1891.
- (11) Barrett, J. A.; Coleman, R. E.; Goldsmith, S. J.; Vallabhajosula, S.; Petry, N. A.; Cho, S.; Armor, T.; Stubbs, J. B.; Maresca, K. P.; Stabin, M. G.; Joyal, J. L.; Eckelman, W. C.; Babich, J. W. First-in-Man Evaluation of 2 High-Affinity PSMA-Avid Small Molecules for Imaging Prostate Cancer. *J. Nucl. Med.* **2013**, *54*, 380–387.
- (12) Maresca, K. P.; Hillier, S. M.; Lu, G.; Marquis, J. C.; Zimmerman, C. N.; Eckelman, W. C.; Joyal, J. L.; Babich, J. W. Small Molecule Inhibitors of PSMA Incorporating Technetium-99m for Imaging Prostate Cancer: Effects of Chelate Design on Pharmacokinetics. *Inorg. Chim. Acta* **2012**, *389*, 168–172.
- (13) Nedrow-Byers, J. R.; Moore, A. L.; Ganguly, T.; Hopkins, M. R.; Fulton, M. D.; Benny, P. D.; Berkman, C. E. PSMA-Targeted SPECT Agents: Mode of Binding Effect on in Vitro Performance. *Prostate* **2012**, *73*, 355–362.
- (14) Lu, G.; Maresca, K. P.; Hillier, S. M.; Zimmerman, C. N.; Eckelman, W. C. J.; Babich, J. L. Synthesis and SAR of ^{99m}Tc /Re-Labeled Small Molecule Prostate Specific Membrane Antigen Inhibitors with Novel Polar Chelates. *Biorg. Med. Chem. Lett.* **2013**, *23*, 1557–1563.
- (15) Nedrow-Byers, J. R.; Jabbes, M.; Jewett, C.; Ganguly, T.; He, H.; Liu, T.; Benny, P.; Bryan, J. N.; Berkman, C. E. A Phosphoramidate-Based Prostate-Specific Membrane Antigen-Targeted SPECT Agent. *Prostate* **2012**, *72*, 904–912.
- (16) Banerjee, S. R.; Foss, C. A.; Castanares, M.; Mease, R. C.; Byun, Y.; Fox, J. J.; Hilton, J.; Lupold, S. E.; Kozikowski, A. P.; Pomper, M. G. Synthesis and Evaluation of Technetium-99m- and Rhenium-Labeled Inhibitors of the Prostate-Specific Membrane Antigen (PSMA). *J. Med. Chem.* **2008**, *51*, 4504–4517.
- (17) Kularatne, S. A.; Zhou, Z.; Yang, J.; Post, C. B.; Low, P. S. Design, Synthesis, and Preclinical Evaluation of Prostate-Specific Membrane Antigen Targeted (^{99m}Tc -Radioimaging Agents. *Mol. Pharmaceutics* **2009**, *6*, 790–800.
- (18) Zhang, Y.; DiFilipp, F.; Doke, A.; Huang, J.; Heston, W.; Huang, S. Preliminary Micro-SPECT and Biodistribution Study of a Novel ^{99m}Tc -Labeled PSMA Tracer Derived from RBI1033. *JNM Mtg. Abstr.* **2012**, *53* (Suppl 1), 1661.
- (19) Mindt, T. L.; Muller, C.; Melis, M.; de Jong, M.; Schibli, R. “Click-to-Chelate”: In Vitro and in Vivo Comparison of a ^{99m}Tc - $(\text{CO})_3$ -labeled N(τ)-Histidine Folate Derivative with its Isostructural, Clicked 1,2,3-Triazole Analogue. *Bioconjugate Chem.* **2008**, *19*, 1689–1695.
- (20) Huisgen, R. 1,3-Dipolar Cycloadditions. Past and Future. *Angew. Chem., Int. Ed.* **1963**, *2*, 565–598.
- (21) Rostovtsev, V. V.; Green, L. G.; Fokin, V. V.; Sharpless, K. B. A Stepwise Huisgen Cycloaddition Process: Copper(I)-Catalyzed Regioselective “Ligation” of Azides and Terminal Alkynes. *Angew. Chem., Int. Ed. Engl.* **2002**, *41*, 2596–2599.
- (22) Banerjee, S. R.; Pullambhatla, M.; Byun, Y.; Nimmagadda, S.; Foss, C. A.; Green, G.; Fox, J. J.; Lupold, S. E.; Mease, R. C.; Pomper, M. G. Sequential SPECT and Optical Imaging of Experimental Models of Prostate Cancer with a Dual Modality Inhibitor of the Prostate-Specific Membrane Antigen. *Angew. Chem., Int. Ed. Engl.* **2011**, *50*, 9167–9170.
- (23) Lazarova, N.; James, S.; Babich, J. W.; Zubieta, J. A Convenient Synthesis, Chemical Characterization and Reactivity of $[\text{Re}(\text{CO})_3(\text{H}_2\text{O})_3]\text{Br}$: The Crystal and Molecular Structure of $[\text{Re}(\text{CO})_3(\text{CH}_3\text{CN})_2]\text{Br}$. *Inorg. Chem. Commun.* **2004**, *7*, 1023–1026.
- (24) Luyt, L. G.; Jenkins, H. A.; Hunter, D. H. An N_2S_2 Bifunctional Chelator for Technetium-99m and Rhenium: Complexation, Conjugation, and Epimerization to a Single Isomer. *Bioconjugate Chem.* **1999**, *10*, 470–479.
- (25) Banerjee, S. R.; Pullambhatla, M.; Byun, Y.; Nimmagadda, S.; Green, G.; Fox, J. J.; Horti, A.; Mease, R. C.; Pomper, M. G. Ga-68-Labeled Inhibitors of Prostate-Specific Membrane Antigen (PSMA) for Imaging Prostate Cancer. *J. Med. Chem.* **2010**, *53*, 5333–5341.
- (26) Wang, Y.; Liu, G.; Hnatowich, D. J. Methods for MAG3 Conjugation and ^{99m}Tc Radiolabeling of Biomolecules. *Nature Protoc.* **2006**, *1*, 1477–1480.
- (27) Greenland, W. E.; Howland, K.; Hardy, J.; Fogelman, I.; Blower, P. J. Solid-Phase Synthesis of Peptide Radiopharmaceuticals Using Fmoc-N-epsilon-(Hynic-Boc)-lysine, a Technetium-Binding Amino Acid: Application to ^{99m}Tc -Labeled Salmon Calcitonin. *J. Med. Chem.* **2003**, *46*, 1751–1757.

- (28) Olszewski, R. T.; Bukhari, N.; Zhou, J.; Kozikowski, A. P.; Wroblewski, J. T.; Shamimi-Noori, S.; Wroblewska, B.; Bzdega, T.; Vicini, S.; Barton, F. B.; Neale, J. H. NAAG Peptidase Inhibition Reduces Locomotor Activity and Some Stereotypes in the PCP model of Schizophrenia via Group II mGluR. *J. Neurochem.* **2004**, *89*, 876–885.
- (29) Silver, D. A.; Pellicer, I.; Fair, W. R.; Heston, W. D.; Cordon-Cardo, C. Prostate-Specific Membrane Antigen Expression in Normal and Malignant Human Tissues. *Clin. Cancer Res.* **1997**, *3*, 81–85.
- (30) Jackson, P. F.; Cole, D. C.; Slusher, B. S.; Stetz, S. L.; Ross, L. E.; Donzanti, B. A.; Trainor, D. A. Design, Synthesis, and Biological Activity of a Potent Inhibitor of the Neuropeptidase N-Acetylated Alpha-Linked Acidic Dipeptidase. *J. Med. Chem.* **1996**, *39*, 619–622.
- (31) Bartholoma, M.; Valliant, J.; Maresca, K. P.; Babich, J.; Zubieta, J. Single Amino Acid Chelates (SAAC): A Strategy for the Design of Technetium and Rhenium Radiopharmaceuticals. *Chem. Commun.* **2009**, 493–512.
- (32) Banerjee, S. R.; Maresca, K. P.; Francesconi, L.; Valliant, J.; Babich, J. W.; Zubieta, J. New Directions in the Coordination Chemistry of ^{99m}Tc : A Reflection on Technetium Core Structures and a Strategy for New Chelate Design. *Nucl. Med. Biol.* **2005**, *32*, 1–20.
- (33) Jurisson, S. S.; Lydon, J. D. Potential Technetium Small Molecule Radiopharmaceuticals. *Chem. Rev.* **1999**, *99*, 2205–2218.
- (34) Shi, J.; Kim, Y. S.; Chakraborty, S.; Jia, B.; Wang, F.; Liu, S. Mercaptoacetyl-glycylglycyl (MAG(2)) as a Bifunctional Chelator for (^{99m}Tc)-Labeling of Cyclic RGD Dimers: Effect of Technetium Chelate on Tumor Uptake and Pharmacokinetics. *Bioconjugate Chem.* **2009**, *20*, 1559–1568.
- (35) Liu, S.; Edwards, D. S.; Looby, R. J.; Poirier, M. J.; Rajopadhye, M.; Bourque, J. P.; Carroll, T. R. Labeling Cyclic Glycoprotein IIb/IIIa Receptor Antagonists with ^{99m}Tc by the Preformed Chelate Approach: Effects of Chelators on Properties of [^{99m}Tc]Chelator–Peptide Conjugates. *Bioconjugate Chem.* **1996**, *7*, 196–202.
- (36) Rao, T. N.; Adhikesavalu, D.; Camerman, A.; Fritzberg, R. A. Technetium(V) and Rhenium(V) Complexes of 2,3-Bis-(mercaptoacetamido)propanoate. Chelate Ring Stereochemistry and Influence on Chemical and Biological Properties. *J. Am. Chem. Soc.* **1990**, *112*, 5798–5804.
- (37) Leamon, C. P.; Parker, M. A.; Vlahov, I. R.; Xu, L. C.; Reddy, J. A.; Vetzal, M.; Douglas, N. Synthesis and Biological Evaluation of EC20: A New Folate-Derived, (^{99m}Tc)-Based Radiopharmaceutical. *Bioconjugate Chem.* **2002**, *13*, 1200–1210.
- (38) Rovenska, M.; Hlouchova, K.; Sacha, P.; Mlcochova, P.; Horak, V.; Zamecnik, J.; Barinka, C.; Konvalinka, J. Tissue Expression and Enzymologic Characterization of Human Prostate Specific Membrane Antigen and its Rat and Pig Orthologs. *Prostate.* **2008**, *68*, 171–182.
- (39) Wallberg, H.; Orlova, A.; Altai, M.; Hosseinimehr, S. J.; Widstrom, C.; Malmberg, J.; Stahl, S.; Tolmachev, V. Molecular Design and Optimization of ^{99m}Tc -labeled Recombinant Affibody Molecules Improves Their Biodistribution and Imaging Properties. *J. Nucl. Med.* **2011**, *52*, 461–469.
- (40) Rusckowski, M.; Qu, T.; Gupta, S.; Ley, A.; Hnatowich, D. J. A Comparison in Monkeys of (^{99m}Tc) Labeled to a Peptide by 4 Methods. *J. Nucl. Med.* **2001**, *42*, 1870–1877.
- (41) Decristoforo, C.; Mather, S. J. Technetium- 99m somatostatin analogues: effect of labelling methods and peptide sequence. *Eur. J. Nucl. Med.* **1999**, *26*, 869–76.
- (42) Decristoforo, C.; Mather, S. J. Preparation, ^{99m}Tc -labeling, and in vitro characterization of HYNIC and N3S modified RC-160 and [Tyr³]octreotide. *Bioconjugate Chem.* **1999**, *10*, 431–438.
- (43) Chang, S. S.; Reuter, V. E.; Heston, W. D.; Bander, N. H.; Grauer, L. S.; Gaudin, P. B. Five Different Anti-Prostate-Specific Membrane Antigen (PSMA) Antibodies Confirm PSMA Expression in Tumor-Associated Neovasculature. *Cancer Res.* **1999**, *59*, 3192–3198.
- (44) Bzdega, T.; Crowe, S. L.; Ramadan, E. R.; Sciarretta, K. H.; Olszewski, R. T.; Ojeifo, O. A.; Rafalski, V. A.; Wroblewska, B.; Neale, J. H. The Cloning and Characterization of a Second Brain Enzyme with NAAG Peptidase Activity. *J. Neurochem.* **2004**, *89*, 627–635.
- (45) Hlouchova, K.; Barinka, C.; Klusak, V.; Sacha, P.; Mlcochova, P.; Majer, P.; Rulisek, L.; Konvalinka, J. Biochemical Characterization of Human Glutamate Carboxypeptidase III. *J. Neurochem.* **2007**, *101*, 682–696.
- (46) Pangalos, M. N.; Neefs, J. M.; Somers, M.; Verhasselt, P.; Bekkers, M.; van der Helm, L.; Fraiponts, E.; Ashton, D.; Gordon, R. D. Isolation and Expression of Novel Human Glutamate Carboxypeptidases with N-Acetylated Alpha-Linked Acidic Dipeptidase and Dipeptidyl Peptidase IV activity. *J. Biol. Chem.* **1999**, *274*, 8470–8483.
- (47) Hlouchova, K.; Barinka, C.; Konvalinka, J.; Lubkowski, J. Structural Insight into the Evolutionary and Pharmacologic Homology of Glutamate Carboxypeptidases II and III. *FEBS J.* **2009**, *276*, 4448–4462.
- (48) Eder, M.; Schafer, M.; Bauder-Wust, U.; Hull, W. E.; Wangler, C.; Mier, W.; Haberkorn, U.; Eisenhut, M. ^{68}Ga -Complex Lipophilicity and the Targeting Property of a Urea-Based PSMA Inhibitor for PET Imaging. *Bioconjugate Chem.* **2012**, *23*, 688–697.
- (49) Afshar-Oromieh, A.; Malcher, A.; Eder, M.; Eisenhut, M.; Linhart, H. G.; Hadaschik, B. A.; Holland-Letz, T.; Giesel, F. L.; Kratochwil, C.; Haufe, S.; Haberkorn, U.; Zechmann, C. M. PET Imaging with a [^{68}Ga]gallium-Labelled PSMA Ligand for the Diagnosis of Prostate Cancer: Biodistribution in Humans and First Evaluation of Tumour Lesions. *Eur. J. Nucl. Med. Mol. Imaging* **2012**, *40*, 486–495.
- (50) Kaiser, E.; Colescott, R. L.; Bossinger, C. D.; Cook, P. I. Color Test for Detection of Free Terminal Amino Groups in the Solid-Phase Synthesis of Peptides. *Anal. Biochem.* **1970**, *34*, 595–598.
- (51) Zhang, Y. M.; Liu, N.; Zhu, Z. H.; Rusckowski, M.; Hnatowich, D. J. Influence of Different Chelators (HYNIC, MAG3 and DTPA) on Tumor Cell Accumulation and Mouse Biodistribution of Technetium- 99m Labeled to Antisense DNA. *Eur. J. Nucl. Med.* **2000**, *27*, 1700–1707.
- (52) Cheng, Y.; Prusoff, W. H. Relationship between the Inhibition Constant (K_i) and the Concentration of Inhibitor which Causes 50% Inhibition (I_{50}) of an Enzymatic Reaction. *Biochem. Pharmacol.* **1973**, *22*, 3099–3108.